Metabolic Engineering 38 (2016) 251–263

Contents lists available at ScienceDirect

Metabolic Engineering

journal homepage: www.elsevier.com/locate/ymben

Original Research Article

Metabolic flux analyses of *Pseudomonas aeruginosa* cystic fibrosis isolates

Michael J. Opperman [a,b], Yair Shachar-Hill [a,*]

[a] Department of Plant Biology, Michigan State University, 612 Wilson Road, East Lansing, MI 48824, USA
[b] Cell and Molecular Biology Graduate Program, Michigan State University, 2240A Biomedical and Physical Sciences Building, East Lansing 48824, USA

ARTICLE INFO

Article history:
Received 22 March 2016
Received in revised form
7 June 2016
Accepted 11 September 2016
Available online 13 September 2016

Keywords:
Cystic Fibrosis
Entner-Doudoroff
Flux balance analysis
Glyoxylate cycle
Metabolic flux analysis
Pseudomonas aeruginosa

ABSTRACT

Pseudomonas aeruginosa is a metabolically versatile wide-ranging opportunistic pathogen. In humans *P. aeruginosa* causes infections of the skin, urinary tract, blood, and the lungs of Cystic Fibrosis patients. In addition, *P. aeruginosa*'s broad environmental distribution, relatedness to biotechnologically useful species, and ability to form biofilms have made it the focus of considerable interest. We used ^{13}C metabolic flux analysis (MFA) and flux balance analysis to understand energy and redox production and consumption and to explore the metabolic phenotypes of one reference strain and five strains isolated from the lungs of cystic fibrosis patients. Our results highlight the importance of the oxidative pentose phosphate and Entner-Doudoroff pathways in *P. aeruginosa* growth. Among clinical strains we report two divergent metabolic strategies and identify changes between genetically related strains that have emerged during a chronic infection of the same patient. MFA revealed that the magnitude of fluxes through the glyoxylate cycle correlates with growth rates.

1. Introduction

Pseudomonas aeruginosa is a gram negative, environmentally widespread, opportunistically pathogenic bacterium; it causes infections, growth inhibition and death in organisms as diverse as amoebas, fungi, plants, nematodes and mammals (Elrod and Braun, 1942; Kerr, 1994; Qureshi et al., 1993; Yorgey et al., 2001). In humans this organism causes infections of the skin, urinary tract, blood, and lung; it is among the most frequent and harmful causes of hospital-acquired infections (Costerton et al., 1999; Cross et al., 1983; Stover et al., 2000). *P. aeruginosa,* which forms biofilms in many environmental and pathogenic situations, is metabolically versatile (Alvarez-Ortega and Harwood, 2007) and intrinsically resistant to many antibiotics; it develops further resistance during chronic infections resulting in treatment failure (Hauser et al., 2011; Livermore, 2002; Lyczak et al., 2002). *P. aeruginosa* infections of the lungs of Cystic Fibrosis (CF) patients are of particular concern.

CF is a genetic disease involving defects in the Cystic Fibrosis Transmembrane conductance Regulator (CFTR) protein that affects an estimated 70000 individuals worldwide (Cohen and Prince, 2012; Gadsby et al., 2006; Riordan et al., 1989; Kerem et al., 1989; Rommens et al., 1989; Sosnay et al., 2013). Defective membrane transport leads to pancreatic insufficiency, diabetes mellitus, bronchiectasis, and chronic bacterial infection of the pulmonary system in adulthood (Manaker and Tino, 1997; Mitchell et al., 2003). While new treatments have begun to change how some CF sub-types are treated (e.g. ivacaftor; Bell et al., 2014), most adults with CF still face chronic bacterial infection, especially by *P. aeruginosa,* leading to the development of highly resistant strains and to the clinical failure of pulmonary treatment, chronic inflammation and progressive damage to the lung, pulmonary failure, and eventual lung transplantation or death in mid-adulthood (Costerton et al., 1999; Hauser et al., 2011; Lyczak et al., 2002; Cohen and Prince, 2012; Bjarnsholt et al., 2009; Breidenstein et al., 2011).

While many studies of *P. aeruginosa* as a pathogen have focused on identifying genetic changes during chronic infection, and on the production of biofilms and virulence factors, much less is known about the system-wide metabolic phenotypes of this and other pathogenic microbes or their physiological adaptations during chronic infections (Costerton et al., 1999; Stover et al., 2000; Bragonzi et al., 2009; Carter et al., 2010; Cheng et al., 1996; Clark et al., 2015; Fothergill et al., 2007; Hogardt and Heesemann, 2013; Lorè et al., 2012; Mavrodi et al., 2001; Mulcahy et al., 2010; Sauer et al., 2004). Omic studies of pathogenic *P. aeruginosa* strains

Abbreviations: CCE, Carbon conversion efficiency; CF, Cystic Fibrosis; EDP, Entner-Doudoroff Pathway; EMPP, Embden Meyerhof Parnas Pathway; FBA, Flux balance analysis; FVA, Flux Variability Analysis; HCA, Hierarchical Clustering Analysis; MFA, Metabolic flux analysis; OPPP, Oxidative Pentose Phosphate Pathway; PCA, Principal Component Analysis; SSr_{es}, sum of squared residuals; TCA, Tricarboxylic acid cycle

* Corresponding author.
E-mail address: yairhill@msu.edu (Y. Shachar-Hill).

http://dx.doi.org/10.1016/j.ymben.2016.09.002
1096-7176/

have described changes at the genomic (Bragonzi et al., 2006; Caballero et al., 2015; Chung et al., 2012; Darch et al., 2015; Jeukens et al., 2014; Markussen et al., 2014; Mena et al., 2008; Rau et al., 2012; Salunkhe et al., 2005), transcriptomic (Salunkhe et al., 2005; Harmer et al., 2013; Hoboth et al., 2009; Huse et al., 2010; Son et al., 2007; Varga et al., 2015), and proteomic (Hoboth et al., 2009; Park et al., 2014; Wu et al., 2015) levels. Such studies have demonstrated numerous changes in the cellular inventory during evolution in the lung environment. To identify which of these many changes are significant for pathogenesis and to measure and predict functional changes in metabolism, a toolbox of network based computational and experimental methods is available. In recent years these tools have begun to be applied to pathogenic microbes, including *P. aeruginosa*.

Constraints-based flux balance analysis (FBA) uses the structure of the metabolic network and the stoichiometries of the reactions of which they are composed to build computational models of metabolism (see Karr et al., 2015; Lewis et al., 2012; Orth et al., 2010 for recent reviews). Such models are used to investigate the potential flows of carbon and other elements as well as cofactor balances and can extend to genome-wide coverage (Lewis et al., 2012; Hyduke et al., 2011). In addition to identifying reactions and conditions essential for growth and improving gene annotations, FBA and related tools allow the prediction of maximal growth rates and the exploration of predicted metabolic flux distributions under the assumption of different optimization strategies ("objective functions", most commonly maximal growth efficiency). FBA investigations of pathogenic organisms have been used to search for novel drug targets and have pointed to potential metabolic targets not affected by current therapeutics, such as amino acid production or fatty acid metabolism (Kim et al., 2014; Larocque et al., 2014; Lee et al., 2009, 2011; Song et al., 2013; Veith et al., 2015; Wang et al., 2014; Kim et al., 2010). Oberhardt and colleagues have constructed a genome-based model of metabolism and transport in *P. aeruginosa* (Oberhardt et al., 2008), and used flux balance analysis (FBA) with transcript data from two CF clinical strains to investigate *P. aeruginosa*'s metabolic capabilities and potential metabolic changes during prolonged infection (Oberhardt et al., 2010). FBA has also been used to identify potential metabolic drug targets during biofilm growth of *P. aeruginosa* (Sigurdsson et al., 2012). To map network-wide metabolic fluxes without assumptions about the strategies or objectives being pursued during cellular metabolism, isotopic labeling experiments are used together with metabolic network models (Niedenführ et al., 2015).

Metabolic flux analysis (MFA) combines ^{13}C labeling results with the growth and uptake measurements used for FBA to yield estimates of carbon fluxes through central metabolism (Kelleher, 2001; Kohlstedt et al., 2010; Wiechert et al., 2001, 1999). Most MFA studies of microbial systems to date have focused on questions related to biotechnology and metabolic engineering, microbial physiology, and gene function (Adebiyi et al., 2015; García Martín et al., 2015; Ghosh et al., 2014; Heux et al., 2014; McAtee et al., 2015). Several recent studies have analyzed the metabolic interactions of pathologically relevant bacteria within their host environment (Beste et al., 2013; Götz et al., 2010) and metabolic differences between mutant strains (Bücker et al., 2014). A recent study of pathogenesis related metabolism in *P. aeruginosa* employed MFA to describe 17 uropathogenic strains (Berger et al., 2014).

The combination of FBA and MFA allows the testing of alternative objective functions, and can identify the origins of submaximal growth rates. However there have been surprisingly few studies in which these complementary network flux analysis approaches have been combined (García Martín et al., 2015; Chen et al., 2011; Maier et al., 2009; Montezano et al., 2015; Puchalka et al., 2008; Schuetz et al., 2007; Toya et al., 2010; Williams et al., 2010; Wu et al., 2015). Here we performed FBA analysis together with ^{13}C MFA of one reference and five selected CF pathogenic strains of *P. aeruginosa* to understand energy and redox production and consumption processes and to explore metabolic (in)efficiencies and metabolic phenotypes. Our results highlight the importance of the oxidative pentose phosphate pathway (OPPP) and Entner-Doudoroff Pathway (EDP) in *P. aeruginosa* growth and point to a substantially lower flux around the tricarboxylic acid pathway than has been previously reported for the same reference strain under similar conditions. The differences were explained by the smaller experimental dataset previously used. Among the clinical strains we report two metabolic strategies and identify changes between genetically related strains that have emerged during the course of a chronic infection of the same patient. MFA identified fluxes through the glyoxylate cycle, whose magnitude correlated with growth rates across strains, although this pathway is not predicted by FBA to increase growth efficiency. Finally we compared the degree of relatedness of metabolism among strains obtained in two ways: in the first approach ^{13}C labeling data alone was used, and in the second the fluxes obtained by MFA were compared. While both approaches clearly discriminated among the strains, the patterns of relatedness revealed by labeling data did not correspond to those apparent from the flux analyses.

Table 1
Pseudomonas aeruginosa strains analyzed. LPS, Lipopolysaccharide; PGN, polygalacturan. N/A, not applicable.

Strain	Origin	Related isolates	Relevant characteristics	References
PAO1	Australia Wound Isolate (1955)	N/A	Standard Reference Strain	Stover et al. (2000) Sauer et al. (2004) Mavrodi et al. (2001)
AMT 0023-30	U.S.A. CF – Pediatric Clinical Isolate (~1998)	AMT 0023-34	Persister Cells Present	Mulcahy et al. (2010) Mena et al. (2008)
LES 400	U.K. CF – Adult Clinical Isolate (2003)	Liverpool Epidemic Strains (LES)	Increased Acute Morbidity Risk Decreased Life Expectancy with Infection Pyocyanin Overproduction Alginate Overproduction CF Transmissible	Cheng et al. (1996) Salunkhe et al. (2005) Carter et al. (2010) Jeukens et al. (2014) Fothergill et al. (2007)
AA2 AA43 AA44	Germany CF – Adult Clinical Sequential Isolates (~1998 & ~2003)	AA43, AA44 AA2, AA44 AA2, AA43	Parental strain of AA43, AA44 7.5 years total lung colonization time Increased Acute Morbidity risk Motility defect Protease reduction LPS and PGN changes	Bragonzi et al. (2006, 2009) Lorè et al. (2012)

2. Materials and methods

2.1. Strain selection and culture

Pseudomonas aeruginosa strains are described in Table 1. Strains were chosen that have sequenced genomes, clinical and epidemiological importance, and to include an example of an ancestral and descendant strains (De Soyza et al., 2013). Strains AA2, AA43, AA44, and LES 400 were obtained from the Belgian Co-ordinated Collections of Micro-organisms (Ghent, Belgium; LMG numbers: 27630, 27631, 27632, and 27623 respectively). *Pseudomonas aeruginosa* strain AMT 0023-30 was obtained from Cystic Fibrosis Isolate Core (Seattle, Washington). *Pseudomonas aeruginosa* strain PA01 was obtained from Dr. M. Mulks at Michigan State University. M9 defined minimal media with 22 mmol glucose as the sole carbon source was used as the culture media for all experiments (Sambrook and Russel, 2001). All cultures were pre-cultured from −80 °C frozen stock samples onto M9 media solidified with 1.5% agarose for 24 h at 37 °C. Single colonies were transferred into 30 ml of M9 liquid media in 250 ml Bellco triple baffled shake flasks, incubated at 37 °C and shaken at 120 RPM until stationary phase (12–14 h) before spectrophotometric measurement of cell density as absorbance at 600 nm (OD_{600}) and inoculation of experimental cultures to initial densities of 0.01 OD_{600}. For ^{13}C-labeling experiments and for measurements of uptake and growth rates, cells were cultured in batch mode in shake flasks using either 99.9% (mol/mol) [1-^{13}C] glucose or 20% (mol/mol) [U-^{13}C] glucose and harvested during exponential growth phase.

2.2. Cell and media sample harvest

Cell pellets were collected by centrifugation of cultures at mid-log phase (OD_{600} ≈0.5). 1 ml of culture was centrifuged at 15,000 × *g* for 5 min. The supernatant was removed and 100 µl of 6N HCl was added to the pellet which was stored at −20 °C. Cell pellet sample preparation for amino acid analysis was based on previously reported methods (Chen et al., 2011; Schwender et al., 2003).

2.3. Determination of substrate uptake rates and product secretion

Glucose uptake rates for each strain were determined from 1 ml culture supernatants using at least three biological replicate samples for each of three log phase time points taken at 15 min intervals. After lyophilization, samples were resuspended in 600 µl of 99% D_2O, and then lyophilized and resuspended in 600 µl of 99.9% D_2O. 1H-NMR was performed on an Agilent *DirectDrive2* 500 MHz instrument using an Agilent *OneNMR* Probe with *Protune* for auto-tuning. Spectra were obtained at 500 MHz with a pulse angle of $<45°$, acquisition time of2.05 s, and recycle delay of 2 s. Glucose concentrations relative to the initial 22 mM were determined with reference to 10 mM methylphosphamide added as internal standard. No secreted products were detected in 1H-NMR spectra (data not shown) at significant levels in the media after culture growth for any of the strains. Calculation of glucose uptake rates during exponential growth used the following equation:

$$v = \frac{\mu}{X_i}\frac{C - C_0}{e^{-\mu t} - 1}$$

Where µ is intrinsic growth rate (h^{-1}); C is the concentration of glucose (mM) at time t; X_i is the initial density ($g \cdot DW/L$) of cells; t is time (hours); and v is uptake flux ($mmol/g \cdot DW/h$).

2.4. Determination of CO_2 efflux rates

Cultures were grown, as described above, to early log phase that were sealed with gas-tight caps and incubated for two hours. Due to the high sensitivity and low maximum range of CO_2 detection of the LICOR CO_2measurement, *P. aeruginosa* growth was limited to a low range of optical density for this measurement. The cell density of the culture was measured and growth was stopped by adding 1 ml 6N HCl to the culture, which also converted dissolved bicarbonate to CO_2. Total CO_2 was measured using a LICOR LI-6400with dry CO_2 free air as input into the culture flask at a rate of 500 µl/s. Readings of total CO_2 were recorded over 5 min (1 s time resolution) to allow for removal of CO_2 from the flask. Total CO_2 evolved was measured in at least three replicate cultures with CO_2 levels integrated for total CO_2 efflux. Due to the very small change in OD during the CO_2 measurement period, CO_2 efflux was calculated from total CO_2 evolved per change in time per total change in dry-weight in grams.

2.5. Carbon conversion efficiency calculation

Carbon Conversion Efficiency (CCE) was calculated using two methods. First, CCE were calculated for total carbon of glucose uptake divided by total dry-weight carbon biomass produced. The second method used the measured total dry-weight carbon biomass produced divided by the total dry-weight carbon biomass and CO_2 efflux measured. Values for total dry-weight carbon biomass were assumed to be 50% of dry-weight biomass as reported for *E. coli* by von Stockar and Liu (Von Stockar and Liu, 1999).

2.6. Analysis of amino acid labeling

Cell pellets were suspended in 1 ml of 6N HCl and incubated at 100 °C for 24 h, and dried at 60 °C under a stream of N_2. Amino acids were derivatized using N-Methyl-N-[*tert*-butyldimethyl-silyl] trifluoroacetimide (MTBSTFA, SIGMA-ALDRICH) in a 25 µl pyrimidine and 25 µl 1% MTBSTFA solution incubated at 40 °C for 1 h as previously described (Chen et al., 2011; Schwender et al., 2003; Allen et al., 2007). GC-MS analyses of derivatized amino acids were performed on an Agilent 5973GC/quadrupole MS. GC-MS signals were corrected for natural isotope abundance (Schwender et al., 2003). Amino acid fragments used in ^{13}C-MFA were based on reported reliability (Allen et al., 2007). Unlabeled amino acid samples collected were used to confirm the accuracy of natural abundance correction. GC–MS amino acid data was corrected for natural abundance isotopic contents with average values and standard deviation calculated for biological replicates used as model inputs.

2.7. Principal Component Analysis (PCA) and Hierarchical Clustering Analysis (HCA)

GC–MS measured mass fragment mass abundance data for amino acids of strains harvested after growth in 100% 1-C^{13} glucose or20% uniformly labeled (1,2,3,4,5,6-C^{13}) glucose was collected. Amino acid fragments that were measureable in three biological replicates were then processed in MATLAB (2010a, Mathworks, Natick MA, U.S.A.) using the PCA function to produce a principal component analysis (Pearson, 1901). HCA was performed on this data set as well as on fluxes determined by MFA that were normalized to each strain's glucose uptake rate. HCA was implemented in the programming language R using complete linkage criteria using Euclidian distance (Dash et al., 2003).

2.8. ^{13}C Metabolic flux analysis

A carbon isotopic network of *P. aeruginosa* central metabolism was constructed by an approach similar to that previously used for *E. coli* (Chen et al., 2011). The iM01056 FBA model (Oberhardt et al.,

2008) reaction network was simplified by only including carbon atoms of reactants and products, by introducing both net and exchange fluxes for reversible fluxes, by combining linear reaction sequences that do not alter carbon positions, and by condensing secondary metabolic pathways into a growth equation that consumes central metabolic intermediates as precursors to produce cellular biomass as previously defined (Oberhardt et al., 2008; Neidhardt and Edwin Umbarger, 1996). By preserving the architecture of the FBA model, results of FBA and ^{13}C MFA could be directly compared, and ^{13}C MFA results examined by FBA (Chen et al., 2011).

Measured rates of glucose uptake, CO_2 efflux, and ^{13}C labeling patterns in amino acids together with growth rates were used to estimate internal fluxes of central carbon metabolism by fitting flux values to the experimental data using the ^{13}C-FLUX software with DONLP2 as the optimization algorithm as previously described (Wiechert et al., 2001, 1999; Chen et al., 2011). For most labeling data, variation among biological replicates was very small (see Supplemental Data 1); since experimental standard deviations (SDs) are not a reliable estimate of true population SDs when 5 or fewer replicates are analyzed, experimentally observed SD's with low SD's were increased to 2% of mean values for MFA modeling as previously described (Chen et al., 2011). This also avoids excessively constraining modeling results to labeling data at the expense of direct flux measurements and reduces the potential for distortions due to precise but inaccurate mass isomer quantification (Chen et al., 2011). To allow for uncertainties in *P. aeruginosa* biomass compositions, production rates were constrained to be within 50% of the *E. coli* biomass values (Chen et al., 2011).

To minimize the risk that solutions represented local rather than global optimization minima, multiple randomly generated initial fluxes constrained by sampling the feasible solution space were used. First, at least 100 randomly generated feasible starting points that produced optimized fits by the ^{13}C-FLUX program were found. Next, the 10 starting points that yielded the lowest final residuum values were used in the second stage to generate 1000 more starting points by randomly perturbing these starting points to yield 100 new points each. The final, lowest residuum optimized flux values that resulted in the best fit to the data were used. Confidence intervals for flux values were estimated using a Monte Carlo approach to randomly generate values of: biomass, glucose uptake rate, CO_2 efflux rate, and amino acid labeling data for each strain (Schmidt et al., 1999) based on the experimentally determined standard deviations. Randomized values were generated using the excel 2007 RAND function between values of 0 and 1 which then were multiplied by the measured standard deviation of values and then added to the measured average values of the data set with randomized negative data set to zero. At least 20 such datasets were then fitted, as described above to yield best-fit flux maps for each dataset for each strain. These 20 flux value sets were then used to calculate 90% confidence intervals for each flux modeled for each strain. Chi-squared distributions of the sum of square residuums were calculated as described by Antoniewicz et al., (2006).

All MFA computations were performed using the High Performance Computer Center, Michigan State University, using a parallel 1536 core cluster of 192 nodes (two four-core Intel Xeon E5620s at 2.4 GHz with 24 GB of RAM and 250 GB local disk space per node). Global sum of squared residuals (SS_{res}) for each strain is listed in Supplemental Data 2.

2.9. Flux balance analysis

The genome-derived stoichiometric *P. aeruginosa* model iM01056 developed by Oberhardt et al. (2008) was used for FBA. The results of PA01are representative of predicted central metabolism for all the strains studied here since their genomes do not appear to lack any functional central metabolic fluxes (Bragonzi et al., 2009; Mena et al., 2008; Salunkhe et al., 2005). The model was modified to better account for lipid production (see Supplemental Data 3) resulting in a total of 1013 reactions and 875 metabolites. The COBRA Toolbox 2.0 in MATLAB (Mathworks, Natick MA, U.S.A.) implementing the Gurobi 6 optimizer was used for FBA using the objective function of maximal biomass production (Hyduke et al., 2011). FBA simulations used measured glucose uptake rates by strain PA01. To determine the range of fluxes that allow 99% or 90% of the maximal growth rates, the Flux Variability Analysis (FVA) function of the COBRA Toolbox was used (Mahadevan and Schilling, 2003).

3. Results

3.1. Physiological measurements of P. aeruginosa isolates

The physiology, growth and yield of the reference and clinical strains were compared during growth in defined medium to characterize any intrinsic or evolved differences among them. Specific growth rates, final culture density (as a measure of carbon conversion efficiency over the full growth cycle), glucose uptake rates, and CO_2 efflux rates were measured as described in Materials and Methods and are shown in Fig. 1.

The growth rates show a 40% range of values, and both glucose uptake and CO_2 efflux rates show a twofold range across strains. Compared to those reported for uropathogenic *P. aeruginosa* strains grown in an artificial urine medium (Berger et al., 2014), strain LES 400 showed a growth rate as high as or higher than the highest previously reported ($0.96\ h^{-1}$ vs $0.91\ h^{-1}$) and strain AA44 showed a glucose uptake rate as low as or lower than the lowest rate reported in uropathogenic strains ($4.92\ mmol\ gDW^{-1}\ h^{-1}$ vs $5.37\ mmol\ gDW^{-1}\ h^{-1}$). *P. aeruginosa* pathogenic strains display a large range of growth parameters under defined growth conditions pointing to divergent physiological phenotypes. By contrast, the maximum optical densities attained at stationary phase showed no statistically significant differences among strains, indicating that the growth yields over the culture period are similar.

To explore whether final yields are reflected in substrate use efficiencies during growth, Carbon Conversion Efficiency (CCE) was calculated (see methods) during log phase growth using biomass production rates compared to: (a) glucose uptake rates; and (b) CO_2 production rates (See Supplemental Fig. S1). CCE values for both methods are not significantly different for any strain, as seen from the 95% confidence intervals and confirmed by a heteroscedastic two sided t-test ($p > 0.05$).

These results are consistent with the absence of detected secreted products in culture media (closed carbon balance). Previous studies of *P. aeruginosa* and *P. fluorescens* also found no evidence for significant metabolite export during growth in defined simple media (Berger et al., 2014; Lien et al., 2015). The values of CCE% found for these strains (59–72%) are higher than the 52% reported for *E. coli* growing under the same conditions (Chen and Shachar-Hill, 2012). In that case the CCE is lowered by acetate secretion, but the range here is lower than the estimated 86% for *P. fluorescens* (as calculated from reported MFA results; Lien et al., 2015).

3.2. ^{13}C amino acid fingerprinting of P. aeruginosa isolates

To assess whether the diverse pathogenic strains have evolved divergent metabolic phenotypes, ^{13}C labeling data for amino acids from cultures grown to steady state with labeled glucose, were

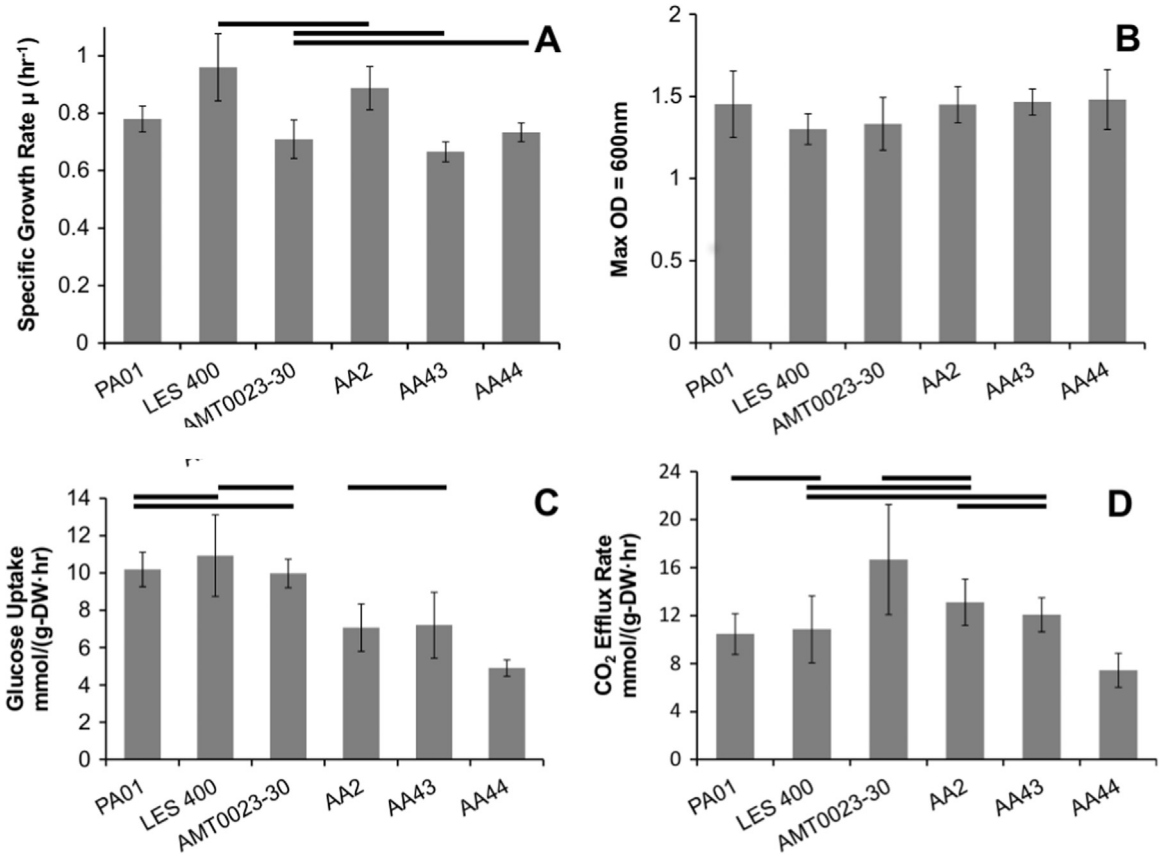

Fig. 1. Growth physiology. (A) Specific growth rates (n=5, AA43 n=4); (B) Final cell densities (OD600, n=3); (C) Glucose uptake rates (AA44 n=7, LES400 n=3, AMT0023-3 n=6, others n=5), and (D) CO_2 efflux rates (AMT0023-30 n=4, AA2 n=5, others n=3). Error bars represent 95% confidence intervals. Horizontal bars in (A), (C), and (D) connect strains that do not show significant difference ($\alpha \leq 0.05$) under two-sided *t*-tests, [no significant differences among strains in (B)].

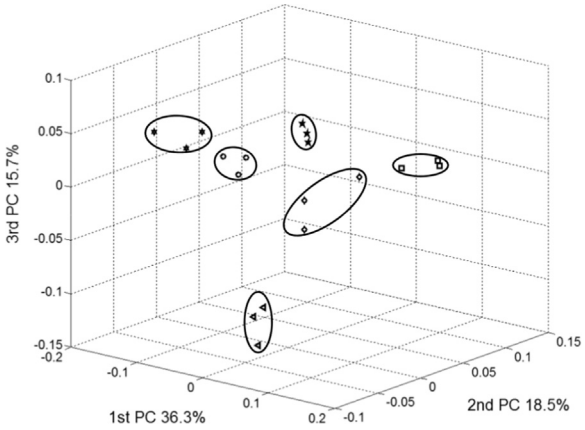

Fig. 2. Discrimination among strains using C^{13} labeling fingerprinting. Principal Component Analysis of the isotopomers of proteinogenic amino acids and their fragments. Steady state labeling was measured in three biological replicates from 100% 1-C^{13} and 20% U_6-C^{13} Glucose experiments (see materials and methods). Strains: AMT0023-30 (circles), AA2 (triangles), AA43 (squares), AA44 (diamonds), LES 400 (pentagrams), and PA01 (hexagrams).

analyzed by Principal Component Analysis (PCA) and Hierarchical Clustering Analysis (HCA; see Supplemental Fig. S2). Both analyses (Fig. 2 and Fig. S2) demonstrate clear differences between strains, with 70% of the variation of the amino acid label data contained in the first three principal components of the PCA. Sample labeled amino acid data used in Fig. 2 can be found in Supplemental Data 1. Both PCA and HCA (see Supplemental Fig. S2) show two groups of strains, one containing AMT 0023-30 and PA01 and the other consisting of AA43, AA2, AA44, and LES 400.

3.3. ^{13}C-MFA and FBA flux maps of reference strain PA01

The ^{13}C MFA flux map of *P. aeruginosa* reference strain (PA01) is shown in Fig. 3. The MFA model, experimental data, and flux tables are given in Supplemental Data 2. The map shows that the flux through the Entner-Doudoroff Pathway (EDP) is equivalent to 60% of the glucose uptake rate. Flux through the decarboxylation step of the oxidative pentose phosphate pathway is equivalent to 85% of the glucose uptake. Published values for aerobic *E. coli* grown under similar conditions show a flux of 25–27% through the OPPP compared to glucose uptake with glycolysis carrying close to 80% of the glucose uptake flux (Chen et al., 2011; Crown et al., 2015). A substantial flux recycles carbon from the OPPP to hexose-monophosphates so that the sum of these fluxes (the total flux from hexose-6-phophate to 6-phosphogluconate) is higher than the glucose uptake rate. *Escherichia coli* studies have also reported cyclic OPPP fluxes under the conditions of this study (Chen et al., 2011; Crown et al., 2015). Little or no net flux was estimated to occur from triose-phosphate to hexose-6-phosphate via the reversible steps of glycolysis. Also noteworthy is the low tri-carboxylic acid (TCA) cycle flux under these aerobic conditions, with significant fluxes estimated though the glyoxylate cycle and anaplerosis from phosphoenolpyruvate carboxylase. Confidence interval calculations of the MFA model indicate that the fluxes are well estimated by the data, with 90% confidence intervals for net fluxes limited to $\pm$10% of flux values in the EDP and OPPP and close to $\pm$20% of fluxes in the TCA cycle.

Flux balance analysis of *Pseudomonas aeruginosa* strain PA01 was performed using a modified genome-derived model (see methods) together with the glucose uptake rate measured for PA01. A predicted flux map based on maximum growth efficiency

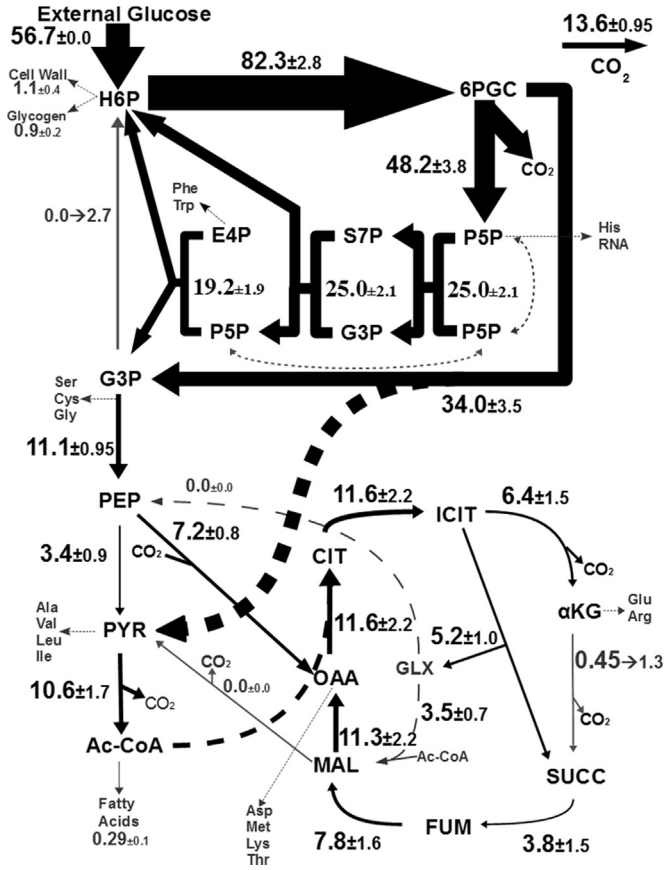

Fig. 3. ^{13}C MFA flux map. Strain PA01 was grown in defined minimal media with either 100% 1-C^{13} or 20% U$_6$-C^{13} Glucose (n=3 replicates for each substrate) to steady state labeling during exponential growth. Labeling and external fluxes were measured and modeled as described in materials and methods. Arrow thicknesses are proportional to net fluxes. Numbers represent net carbon fluxes in units of c-mmol flux/(gDW hr); values are given ± 90% confidence intervals (CI). The range of fluxes catalyzed by Aldolase and alpha-ketogluarate dehydrogenase show the optimized model results paired with the upper range of the calculated CI90% as these fluxes are limited to 0 (irreversible). Non-standard or potentially ambiguous abbreviations: 6PGC, 6-phospho-gluconate; G3P,Glyceraldehyde 3-phosphate; H6P, hexose-6-phosphate; P5P, Pentose-5-Phosphate.

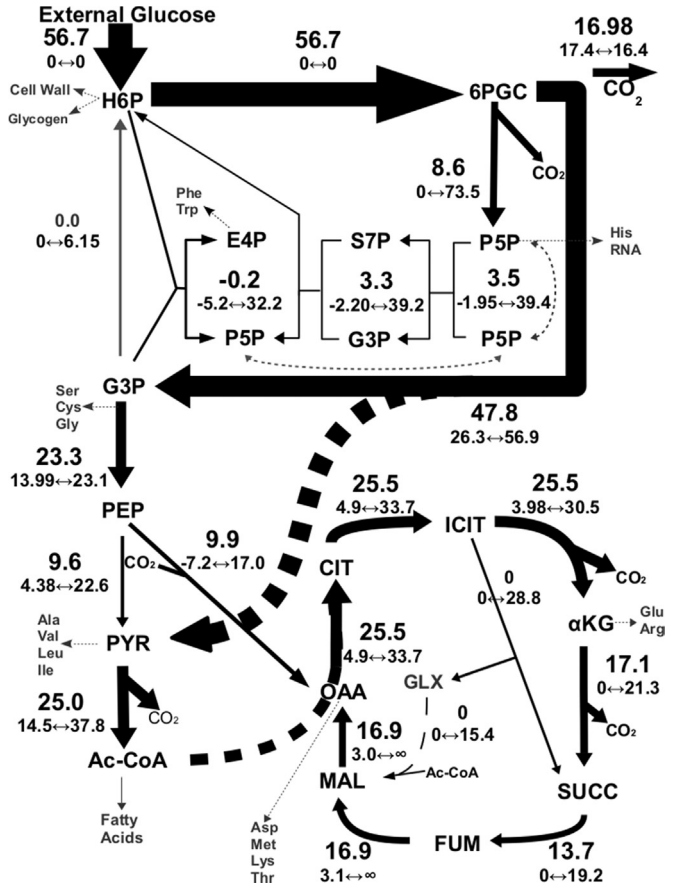

Fig. 4. Flux map from FBA analysis of strain PA01. Uptake of glucose, production of CO_2 and growth rate were used to constrain a stoichiometric genome-derived metabolic model (see materials and methods) with the objective function being maximal growth (corresponding to maximal growth yield on glucose). Numbers are net fluxes as in Fig. 3. Ranges are from flux variability analysis (range of each flux consistent with 99–100% of maximal growth).

(maximal biomass production for the glucose uptake rate) as the objective function is shown in Fig. 4. A listing of the predicted net fluxes for optimal growth is in the supplemental materials (Supplemental Data 3).

The FBA flux map shows several differences from the MFA experimentally based map for PAO1. Cyclic flux in the oxidative pentose phosphate pathway is not seen in the FBA map; instead the majority of the carbon flows through the Entner-Doudoroff pathway and the OPPP decarboxylation flux is predicted to be lower than estimated by MFA. FBA predicts a robust tri-carboxylic acid cycle flux that is not consistent with the fluxes estimated by MFA. FBA predicts maximal growth efficiency (CCE) to be 70%, compared to the 60–65% observed.

To assess whether particular fluxes estimated by MFA are likely to be responsible for the submaximal CCE observed for PA01, flux variability analysis (FVA) was used to determine the ranges of fluxes consistent with 99–100% of maximal predicted. The results are shown in Fig. 3 and Table 2 and predict that near-maximal growth could be sustained with a large range of individual fluxes. For example the first committed step of the OPPP (decarboxylation of6-phosphogluconate) can have 0–130% of the predicted optimal value. The MFA map for PA01 shows several net fluxes outside the range defined by FVA for near-optimal growth: (A) G3P to PEP flux is estimated by MFA at 20% of glucose uptake with a range of 49–81%calculated by FVA;(B) pyruvate to Ac-CoA and CO_2 (19% of glucose uptake in MFA vs 51–133% from VFA); and (C) PEP to pyruvate (6% vs. 49–81%).

3.4. *^{13}C-MFA flux results of CF isolates*

To quantify the metabolic differences among strains isolated from the cystic fibrosis lung environment, metabolic flux analysis was conducted on the clinical strains (Table 1). Flux values estimated by MFA are listed in Table 2 (full flux lists can be found in Supplemental Data 2) and net fluxes are displayed relative to the PAO1 flux values in Fig. 5A while B shows flux values relative to the uptake rate of glucose for each strain. This figure demonstrates that CO_2 efflux and phosphoenolpyruvate carboxylase flux rates across all strains are within 30% of the reference strain flux even though glucose uptake rates show a variation of 49–106%. The estimated EDP and TCA cycle fluxes vary widely across strains with 2 fold and 3.5 fold ranges, respectively. The α-ketoglutarate dehydrogenase flux is very low in reference strain PA01, and is highly variable across the other strains Fig. 5A). Finally, it was observed that the flux rate of isocitrate lyase plotted against the measured intrinsic growth rate of all strains showed the greatest linear correlation (0.599 R^2) of flux to growth rate outside of the biomass related synthesis fluxes. This value increased to a R^2 value of 0.982 with the removal of strain AA2's MFA derived flux from this data set (see Supplemental Fig. S3).

Table 2
Net and exchange (Xch) fluxes determined by 13C MFA (see materials and methods) with 90% confidence intervals. Residuum is the minimal sum-of-squares optimized value found using C13-Flux. Abbreviations as for Fig. 3.

Strain	**PA01**		**LES 400**		**AMT 0023-30**		**AA2**		**AA43**		**AA44**	
Flux	**Net Flux**	**Xch Flux**	**Net Flux**	**Xch Flux**	**Net Flux**	**Xch Flux**	**Net Flux**	**Xch Flux**	**Net Flux**	**Xch Flux**	**Net Flux**	**Xch Flux**
Glucose Uptake	9.45 ± 0.00	N/A	10.05 ± 0.22	N/A	9.25 ± 0.24	N/A	6.96 ± 0.23	N/A	5.79 ± 0.23	N/A	4.80 ± 0.11	N/A
H6P → 6PGC	13.71 ± 0.47	N/A	14.42 ± 0.52	N/A	12.69 ± 0.42	N/A	6.34 ± 0.28	N/A	5.34 ± 0.43	N/A	5.75 ± 0.20	N/A
6PGC → G3P + PYR	5.67 ± 0.57	N/A	10.13 ± 0.65	N/A	11.35 ± 0.55	N/A	5.96 ± 0.21	N/A	4.97 ± 0.25	N/A	3.26 ± 0.11	N/A
G3P → PEP	3.69 ± 0.32	0.84 ± 0.02	2.87 ± 0.37	0.86 ± 0.03	2.19 ± 0.43	0.86 ± 0.04	4.36 ± 0.20	0.81 ± 0.03	3.62 ± 0.22	0.95 ± 0.04	2.31 ± 0.07	0.78 ± 0.04
PEP → PYR	1.14 ± 0.31	0.56 ± 0.03	0.75 ± 0.29	0.57 ± 0.03	−0.24 ± 0.44	0.58 ± 0.02	2.19 ± 0.19	0.53 ± 0.02	1.64 ± 0.17	0.44 ± 0.03	0.97 ± 0.10	0.45 ± 0.02
2 G3P → H6P	0.00 ± 0.45	N/A	2.85 ± 0.54	N/A	3.44 ± 0.51	N/A	0.00 ± 0.00	N/A	0.00 ± 0.00	N/A	0.00 ± 0.04	N/A
6PGC → 2 R5P	8.04 ± 0.63	N/A	4.29 ± 0.72	N/A	1.34 ± 0.46	N/A	0.38 ± 0.23	N/A	0.36 ± 0.37	N/A	2.48 ± 0.18	N/A
2 R5P → S7P + G3P	2.50 ± 0.21	0.51 ± 0.09	1.20 ± 0.23	0.47 ± 0.03	0.31 ± 0.15	0.29 ± 0.05	−0.01 ± 0.08	0.35 ± 0.02	0.02 ± 0.12	0.28 ± 0.04	0.72 ± 0.06	0.20 ± 0.05
S7P + G3P → R5P + E4P	2.50 ± 0.21	0.95 ± 0.05	1.20 ± 0.23	0.95 ± 0.00	0.31 ± 0.15	0.95 ± 0.00	−0.01 ± 0.08	0.95 ± 0.00	0.02 ± 0.12	0.95 ± 0.00	0.72 ± 0.06	0.95 ± 0.00
R5P + E4P → H6P + G3P	2.13 ± 0.21	0.17 ± 0.07	0.77 ± 0.22	0.00 ± 0.01	0.00 ± 0.14	0.00 ± 0.04	−0.28 ± 0.09	0.28 ± 0.06	−0.22 ± 0.12	0.14 ± 0.06	0.50 ± 0.05	0.14 ± 0.04
PYR → CO_2 + AcCoA	3.54 ± 0.52	N/A	6.84 ± 0.45	N/A	8.14 ± 0.38	N/A	5.41 ± 0.28	N/A	4.31 ± 0.31	N/A	2.17 ± 0.16	N/A
OAA + AcCoA → CIT	1.93 ± 0.37	N/A	3.76 ± 0.28	N/A	6.86 ± 0.56	N/A	4.14 ± 0.30	N/A	3.49 ± 0.31	N/A	1.13 ± 0.13	N/A
CIT → ICIT	1.93 ± 0.37	N/A	3.76 ± 0.28	N/A	6.86 ± 0.56	N/A	4.14 ± 0.30	N/A	3.49 ± 0.31	N/A	1.13 ± 0.13	N/A
ICIT → αKG + CO_2	1.07 ± 0.25	0.00 ± 0.11	1.40 ± 0.16	0.21 ± 0.09	6.20 ± 0.72	0.00 ± 0.06	3.62 ± 0.35	0.05 ± 0.09	3.30 ± 0.38	0.00 ± 0.10	0.48 ± 0.14	0.00 ± 0.06
αKG → SUCC + CO_2	0.09 ± 0.27	N/A	0.19 ± 0.15	N/A	5.32 ± 0.71	N/A	2.85 ± 0.41	N/A	2.68 ± 0.37	N/A	0.01 ± 0.12	N/A
SUCC → FUM	0.96 ± 0.38	0.01 ± 0.00	2.55 ± 0.23	0.01 ± 0.00	5.98 ± 0.55	0.01	3.37 ± 0.32	0.01 ± 0.00	2.88 ± 0.30	0.01 ± 0.00	0.66 ± 0.09	0.01 ± 0.00
FUM C_1 → MAL C_1	0.97 ± 0.20	0.95 ± 0.15	1.89 ± 0.11	0.00 ± 0.15	3.39 ± 0.28	0.16 ± 0.13	2.03 ± 0.16	0.69 ± 0.15	1.72 ± 0.16	0.67 ± 0.11	0.60 ± 0.05	0.01 ± 0.13
FUM C_1 → MAL C_4	0.97 ± 0.20	0.95 ± 0.15	1.89 ± 0.11	0.00 ± 0.15	3.39 ± 0.28	0.16 ± 0.13	2.03 ± 0.16	0.69 ± 0.15	1.72 ± 0.16	0.67 ± 0.11	0.60 ± 0.05	0.01 ± 0.13
MAL → OAA	2.81 ± 0.54	0.95 ± 0.15	6.13 ± 0.39	0.95 ± 0.00	7.43 ± 0.43	0.95 ± 0.06	4.58 ± 0.29	0.95 ± 0.06	3.63 ± 0.31	0.95 ± 0.08	1.86 ± 0.15	0.95 ± 0.06
ICIT → GLX + SUCC	0.86 ± 0.16	N/A	2.36 ± 0.20	N/A	0.66 ± 0.24	N/A	0.52 ± 0.18	N/A	0.20 ± 0.16	N/A	0.65 ± 0.08	N/A
GLX + AcCoA → MAL	0.86 ± 0.16	N/A	2.36 ± 0.20	N/A	0.65 ± 0.25	N/A	0.52 ± 0.19	N/A	0.20 ± 0.17	N/A	0.65 ± 0.09	N/A
MAL → PYR + CO_2	0.00 ± 0.00	0.00 ± 0.10	0.00 ± 0.00	0.76 ± 0.08	0.00 ± 0.00	0.92 ± 0.06	0.00 ± 0.01	0.79 ± 0.04	0.00 ± 0.00	0.82 ± 0.08	0.00 ± 0.00	0.40 ± 0.06
PEP + CO_2 → OAA	1.81 ± 0.19	0.00 ± 0.05	1.25 ± 0.16	0.00 ± 0.02	1.82 ± 0.28	0.00 ± 0.04	1.62 ± 0.17	0.17 ± 0.07	1.50 ± 0.16	0.00 ± 0.08	0.89 ± 0.06	0.00 ± 0.04
2 GLX → PEP	0.00 ± 0.00	0.00 ± 0.03	0.00 ± 0.00	0.00 ± 0.02	0.00 ± 0.05	0.00 ± 0.01	0.00 ± 0.06	0.00 ± 0.00	0.00 ± 0.01	0.00 ± 0.00	0.00 ± 0.01	0.00 ± 0.01
CO_2 Efflux	13.62 ± 0.95	N/A	14.13 ± 0.77	N/A	21.67 ± 1.76	N/A	13.29 ± 0.61	N/A	11.58 ± 0.78	N/A	7.82 ± 0.55	N/A
Final Residuum	182.27		142.11		99.88		73.72		72.75		86.43	
χ^2 Calculated *p*-values	1.44E − 02		1.06E − 02		1.88E − 06		8.72E − 12		1.62E − 11		8.89E − 09	

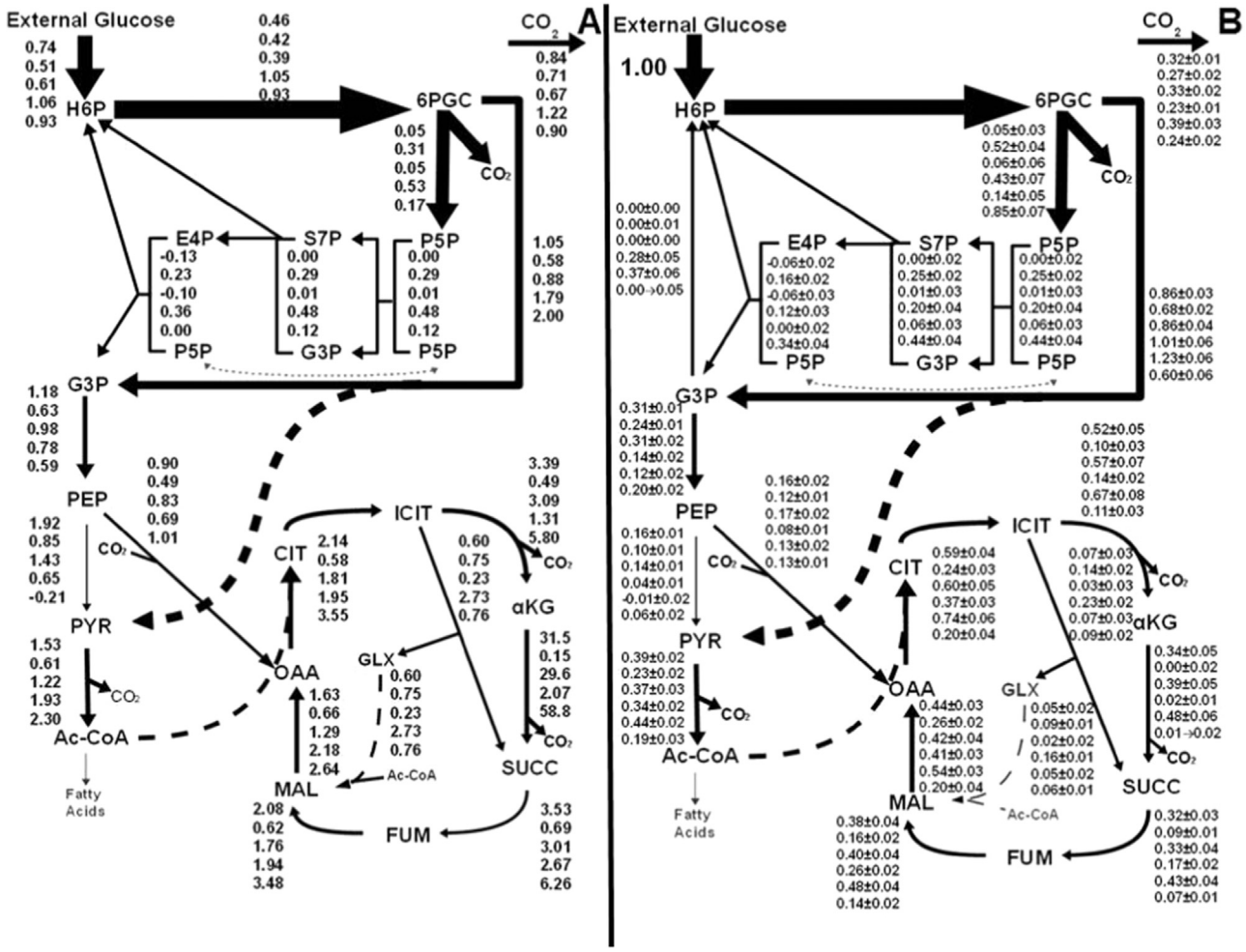

Fig. 5. ^{13}C-MFA flux maps of *P. aeruginosa* cystic fibrosis clinical isolates. (A) Net fluxes relative to those of the reference strain, PA01. (B) MFA determined fluxes (moles of C) in experimental strains relative to the carbon molar flux of glucose uptake. Each flux is expressed with its ±90% confidence intervals. Several arrows were removed in comparison to Fig. 3 due to either low flux in the reference strain (ED7 in A) or zero fluxes seen in reaction for all strains. From top to bottom: AA2, AA44, AA43, LES400, AMT0023-30, and PA01 (B only). Arrow weights of figure do not quantitatively correspond to flux sizes. The reactions catalyzed by Aldolase and alpha-ketogluarate dehydrogenase (strain PA01) show the optimized model results paired with the upper range of the calculated CI90% as modeled confidence interval results are limited to a flux of zero and notation used for other reactions would imply a reversible flux.

3.5. Determination of metabolic phenotypes

Hierarchical Clustering Analysis (HCA) of MFA flux values normalized to measured glucose uptake rates (Fig. 6) separated strains into two groups with distinct metabolic strategies. LES 400, AA44, and PA01 were in one group and AA2, AA43, and AMT 0023-30 were in the other. The group containing LES 400, PA01, and AA44 shows little or no decarboxylation of 2-oxoglutarate (α-ketoglutarate, in the TCA cycle) and much higher OPPP fluxes in comparison to the AA2, AMT0023-30, and AA43 group. To investigate the differences that underlie these groupings, the ratios of fluxes through key pathways are shown in Table 3.

These ratios were based on major branch points such as between the TCA and Glyoxylate cycles and EDP:OPPP as well as on alternate sources of co-factors. Total NAD(P)H and ATP production rates are also shown. This analysis points to the ratios GLX/TCA, ED/TCA, OPPP/ED and OPPP/TCA being markedly different between the two flux phenotypes discriminated by HCA (Fig. 6). A calculation of flux ratios derived from FBA using a maximized biomass production objective function is included, showing that with the exception of the GLX/TCA flux, maximal growth fluxes fall within the variation across strains while none of the strains shows flux partitioning predicted by maximal growth. Flux ratios derived from MFA aerobic *E. coli* measures (Chen et al., 2011) also are included, with EMPP used in place of EDP, for comparison to another gram-negative bacteria grown under similar conditions. While the *E. coli* is closer in its flux ratios to strains LES 400, PA01, and AA44, Table 3 clearly demonstrates very different energy utilization strategies for glucose consumption, with a net negative total direct ATP production in *P. aeruginosa* compared to a positive ATP production in *E. coli*. *P. aeruginosa* growth is also significantly higher than *E. coli* under similar conditions. A related species, *P. fluorescens*, MFA (Lien et al., 2015) under similar conditions is also included in this table, demonstrating metabolic differences between alginate non-producing wild-type (SBW25) and an alginate operon induced but non-alginate producing mutant (mucA-ΔalgC; Borgos et al., 2013).

4. Discussion

Many studies of *Pseudomonas aeruginosa* have focused on identifying genetic changes (Bragonzi et al., 2006; Jeukens et al., 2014; Mena et al., 2008), production of biofilm (Mavrodi et al., 2001; Ma et al., 2009; Van Alst et al., 2007; Wagner and Iglewski, 2008), variation in biofilm components (Hogardt and Heesemann, 2013; Mulcahy et al., 2010; Stewart and Franklin, 2008), biofilm dispersal (Sauer et al., 2004; McDougald et al., 2011), virulence

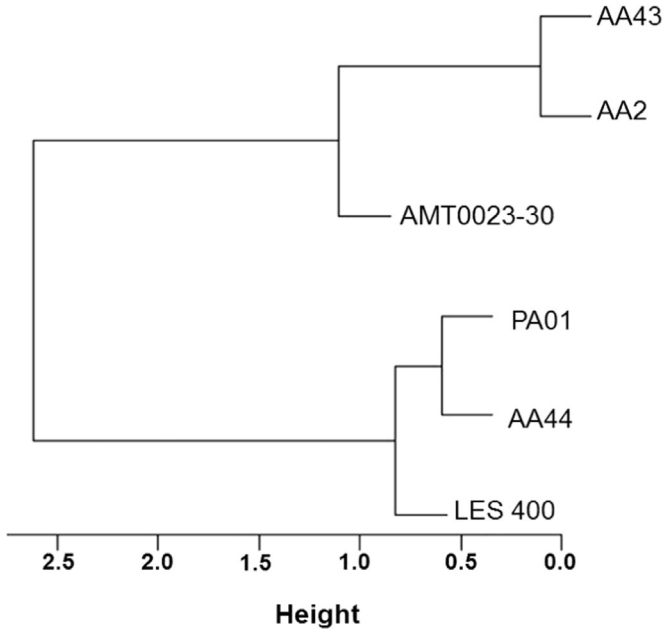

Fig. 6. Discrimination of metabolic phenotypes among *P. aeruginosa* strains. Hierarchical Clustering Analysis using MFA derived flux values was employed to identify two main groupings as discussed in the text.

factor production (Bragonzi et al., 2009; Carter et al., 2010; Fothergill et al., 2007; Lorè et al., 2012; Salunkhe et al., 2005), understanding antibiotic resistance (Breidenstein et al., 2011), and identifying pathogenic and phenotypic differences between environmental isolates and pathogenic isolates (Alonso et al., 1999; Head and Yu, 2004). Quantifying metabolic fluxes across strains can show whether the genetic and physiological differences correspond to metabolic flux patterns. This study provides the first direct evidence of two distinct metabolic phenotypes among clinical isolates from cystic fibrosis infections by *P. aeruginosa*, a high TCA and EDP with low OPPP flux metabolic phenotype and a high OPPP low TCA flux metabolic phenotype.

4.1. Previous MFA study of P. aeruginosa

An earlier MFA study of uropathogenic *P. aeruginosa* strains reported a significantly different map of central metabolic fluxes for the PAO1 reference strain to the one we observed (Table 2; flux values of Berger et al. data normalized to uptake rate flux can be found in Supplemental Data 2). These include a much smaller carbon flux through the OPPP (1.07 mmol $gDW^{-1}\,h^{-1}$ vs our finding of 8.03 mmol $gDW^{-1}\,h^{-1}$), a larger portion of carbon passing through the EDP (8.24 mmol $gDW^{-1}\,h^{-1}$ vs 5.67 mmol $gDW^{-1}\,h^{-1}$), a substantial TCA cyclic flux (6.42 mmol $gDW^{-1}\,h^{-1}$ vs1.93 mmol $gDW^{-1}\,h^{-1}$), and import of carbon into the TCA cycle from pyruvate and its metabolites with an output flux from the TCA cycle from oxaloacetate to phosphoenolpyruvate (Berger et al., 2014). If this divergence is due to the effects of the media (moderately higher salt content in the earlier study) it would highlight metabolic plasticity in *P. aeruginosa*. The alternative is that experimental/analytical differences account for the flux map discrepancies. Since Berger et al. in keeping with common practice, used a single labeling scheme (100% 1-C^{13} glucose), we repeated our MFA analysis using only the 100% 1-C^{13} glucose labeled amino acid data obtained in this study. This yielded fluxes closer to that reported by Berger et al., with a decreased OPPP decarboxylation flux, and increased fluxes in the TCA cycle and EDP (see Supplemental Data 4). We also tested the effect of removing the measurements of CO_2 efflux rate (which limited this study's MFA CO_2 efflux rate to be between 23 and 39% of glucose uptake rates and which is not measured in most MFA studies). This additional reduction in constraining data resulted in estimated fluxes that are very similar to the one reported by Berger et al. (see Supplemental Data 4). Crown et al. (2015) recently reported that multiple glucose labeling experiments yield better resolution and confidence in ^{13}C MFA of *E. coli* than one labeled isotopomer or one combination of isotopomers. This is consistent with previous label design studies (reviewed in Antoniewicz, 2013), and our observations here and previously (Chen et al., 2011; Chen and Shachar-Hill, 2012; Alonso et al., 2007; Paula Alonso et al., 2010), which also support the value of gas exchange measurements in ^{13}C MFA.

4.2. ^{13}C amino acid fingerprinting and MFA

Due to the generally low throughput of MFA, there have been efforts both to speed up flux analyses (Heux et al., 2014; Junker, 2014), to use ^{13}C labeling patterns in metabolite profile datasets without flux mapping to identify pathway activities (Chokkathukalam et al., 2014) and to correlate differences in steady state labeling of biomass (protein amino acids) with alterations in

Table 3
Flux ratios and cofactor production rates for *P. aeruginosa* strains. The ratios of fluxes at major central metabolic branch points, as discussed in the text, separate the strains into the two groupings shown in Fig. 6. Estimated cofactor production rates are from MFA determined flux maps normalized to the glucose uptake rate for each strain. ATP, substrate level phosphorylation; NADP(H) total cellular NADH + NADPH production. Strains LES 400, PA01, and AA44 show higher flux ratios but lower relative ATP generation rates than strains AA2, AMT 0023-30, and AA43. Flux ratios calculated using: $GLX/TCA = V_{(ICIT\rightarrow GLX+SUCC)}/V_{(OAA+AC\text{-}COA\rightarrow CIT)}$; $ED/TCA = V_{(6PG\rightarrow G3P+PYR)}/V_{(OAA+AC\text{-}COA\rightarrow CIT)}$; $ED/OPPP = V_{(6PG\rightarrow G3P+PYR)}/V_{(P5P+P5P\rightarrow S7P+G3P)}$; $OPPP/TCA = V_{(P5P+P5P\rightarrow S7P+G3P)}/V_{(OAA+AC\text{-}COA\rightarrow CIT)}$. These results show the differences in energy turnover, with strain AMT0023-30 being the highest in energy produced per glucose uptake and ATP production per unit of growth. NADPH consumption related to biosynthesis estimated from FBA values were removed from the total NAD(P)H pool before ATP equivalent calculation.

	Growth rate (μ)	GLX/TCA	ED/TCA	OPPP/ED	OPPP/TCA	NAD(P)H	ATP	FADH2	Respiratory ATP synthesis
PA01 FBA	0.85	0.00	1.87	0.07	0.14	38.71	−2.82	3.42	99.11
LES 400	0.96 ± 0.12	0.63 ± 0.11	2.69 ± 0.10	0.20 ± 0.20	0.53 ± 0.21	39.35 ± 2.54	−9.12 ± 0.67	2.55 ± 0.23	93.09 ± 0.97
PA01	0.78 ± 0.05	0.45 ± 0.27	2.93 ± 0.22	0.74 ± 0.13	2.16 ± 0.21	38.86 ± 2.48	−8.21 ± 0.58	0.96 ± 0.38	90.36 ± 1.34
AA44	0.73 ± 0.03	0.57 ± 0.17	2.89 ± 0.12	0.37 ± 0.09	1.06 ± 0.14	17.69 ± 0.98	−3.81 ± 0.33	0.66 ± 0.09	41.40 ± 0.66
AA2	0.89 ± 0.08	0.13 ± 0.36	1.44 ± 0.08	0.00 ± 9.79	0.00 ± 9.79	29.10 ± 1.99	−1.91 ± 0.83	3.37 ± 0.32	75.88 ± 1.15
AMT 0023-30	0.71 ± 0.07	0.10 ± 0.38	1.65 ± 0.09	0.05 ± 0.50	0.07 ± 0.51	44.41 ± 3.41	−4.17 ± 1.39	5.98 ± 0.55	115.82 ± 1.72
AA43	0.67 ± 0.03	0.06 ± 0.82	1.42 ± 0.10	0.01 ± 5.81	0.01 ± 5.81	24.71 ± 2.38	−1.47 ± 0.83	2.88 ± 0.30	64.62 ± 1.23
P. fluorescens SBW25	0.04	0	0.59 ± 0.00	0.35 ± 40.61	0.21 ± 40.61	15.03 ± 1.56	0.20 ± 2.04	3.06 ± 100.00	42.36 ± 102
P. fluorescens mucA-ΔalgC	0.04	0.11 ± 0.0	0.44 ± 0.00	1.34 ± 0.00	0.59 ± 0.00	9.19 ± 1.86	2.45 ± 3.80	1.47 ± 100.20	27.63 ± 212
E. coli aerobic	0.58 ± 0.01	0.14 ± 0.79	5.14 ± 4.05[#]	0.33 ± 0.03[#]	1.68 ± 0.29	31.89 ± 2.32	10.77 ± 1.93	0.27 ± 0.33	90.90 ± 3.98

[#] Designates values for which the EMP pathway was used instead of the ED.

particular fluxes among knockout mutants or different substrate use (Zamboni and Sauer, 2004). Here, we examined whether relatedness of strains in their overall labeling patterns was linked to relatedness in flux maps, which would be particularly valuable in flux phenotype screening of multiple strains. Our results show that while strains can be reliably separated using amino acid labeling patterns, the nature and degree of metabolic differences cannot be straightforwardly inferred.

4.3. ^{13}C-MFA metabolic phenotypes comparison to genotypes

Previous sequencing work creates the potential to assess genotype-phenotype relationships. Strain LES 400 was genomically compared to strain PA01, identifying multiple potentially significant genetic differences between these strains (Jeukens et al., 2014)). Under the conditions of this study, the genomic differences did not cause large changes in the flux patterns. Previous study of the closely related strains AA2, AA43, and AA44, identified AA44 as being different in its non-mucoid character (Bragonzi et al., 2009). Here we observed substantial flux pattern differences between AA2 and AA43 on the one hand and AA44 on the other under conditions where no significant exopolysaccharide production was detected. Strain AMT0023-30, which was characterized as having persister cells (Mulcahy et al., 2010) segregated with these mucoid strains. Persister cells are often associated with biofilm formation (Lewis, 2010) so the flux differences observed here may be functionally related to differences between strains that for biofilms versus non-biofilm formers. A MFA study of a wild-type strain of *P. fluorescens* and a mutant that has induced alginate production signaling with corresponding deletion of a necessary enzyme for alginate production strain reported flux map differences that resemble the two metabolic phenotypes seen in this study between the two phenotypic groups: high TCA and EDP with low OPPP flux in one; and low TCA and high OPPP flux in the other, which may be indicative of a pro-biofilm production metabolic phenotype in several of these strains (Lien et al., 2015). An FBA study of *Neisseria meningitidis*, another species lacking a complete EMPP, also predicted that these two extremes in TCA and OPPP flux can exist (Baart et al., 2008). We note that the flux phenotypes of strains AA43 and AA44 show divergent metabolic adaptations compared to their shared ancestor: strain AA2. These changes may be due to divergent niche specialization in the lung due to different oxygen availability, oxidative stress from immune system attack, or local variation in substrate availability. Both strains show indications of a general increase in the efficiency of converting carbon substrates into biomass. An analysis of a larger number of genotypically-related evolved strains would be of interest to further explore possible divergent metabolic evolution strategies in the lung. Thus different basal metabolic strategies can be observed in related strains after prolonged survival in the cystic fibrosis lung (Lorè et al., 2012).

4.4. Metabolism and pathogenicity

Several studies have investigated the importance and interplay between metabolism and pathogenicity. The Entner-Doudoroff Pathway (EDP) is a well conserved pathway in the *Pseudomonas* genus (Kessie, 1984; Romano and Conway, 1996), whose members lack a complete EMPP, and has been shown to be preferentially utilized by glucose consuming marine bacteria and to correlate with oxidative stress tolerance (Klingner et al., 2015). The EDP was postulated to have selective advantages based on the observation of lowered fitness when Fructose-bisphosphate aldolase was introduced in a related species, *Pseudomonas putida* (Chavarría et al., 2013). The EDP has also been argued to have advantages due to lower protein expression requirements and increased NADPH production in comparison to the EMPP (Chavarría et al., 2013; Flamholz et al., 2013). A previous transcriptomics study on sequential CF isolates of *P. aeruginosa* from three separate patients demonstrated no change in expression levels of EDP enzymes, which contrasts with the variability in the carbon flux among the strains investigated here (Hoboth et al., 2009). This study also demonstrates through MFA findings that efficient growth relies on utilization of EDP over the OPPP. Glyceraldehyde-3-phosphate cycling from the EDP has also been discussed in the literature of *Pseudomonas*, with evidence of this occurring in mutants (Kessie, 1984) and alginate label studies in *Pseudomonas mendocina* (Anderson et al., 1987).

Decreases in TCA utilization in pathogenic organisms has also been shown to correspond to changes in virulence. These metabolic changes are associated with increases in survivability and growth within the oxidative environment of activated macrophages in *Salmonella typhiurium* (Abernathy et al., 2013; Bowden et al., 2010), attenuation of virulence in *Salmonella enterica* and *Yersinia pseudotuberculosis* (Bücker et al., 2014; Mercado-Lubo et al., 2009), and decrease in type III secretion system expression in *Y. pseudotuberculosis* and *P. aeruginosa* (Bücker et al., 2014; Dacheux et al., 2002; Wilharm and Heider, 2014). Finally, the glyoxylate shunt has been implicated in pathogenesis of organisms in human disease (Dunn et al., 2009). In addition to upregulation of isocitrate lyase in CF infections (Son et al., 2007), direct evidence of the importance of the glyoxylate shunt in *P. aeruginosa* pathogenicity was shown in a mutant screen, where the knockout of isocitrate lyase prevented infection of alfalfa seedlings and substantially reduced lung infection (Lindsey et al., 2008). Additional evidence has demonstrated a role in the production of hydrogen cyanide, which can be derived from the intermediates of the glyoxylate shunt, by *P. aeruginosa* and impairment in lung function in CF patients (Hagins et al., 2009; Ryall et al., 2008). Here we observed small-to-moderate fluxes through this shunt in all strains, and a significant correlation between this flux and intrinsic growth rate across strains. This pathway activity under conditions when neither fatty acids nor acetate were provided, points to a possible anapleurotic role.

Oxidative stress during chronic infection may explain some of the flux patterns observed. Oxidative bursts are seen in many different organisms' response to bacterial infection (Jain et al., 2009; Kavanagh and Reeves, 2004; Lamb and Dixon, 1997; Lambeth, 2004), and high oxidative stress in cystic fibrosis patients has been well documented (Lagrange-Puget et al., 2004; Ziady and Hansen, 2014). A correlation has been established between oxidative stress and strain diversity in *P. aeruginosa* (Ciofu et al., 2005). Glucose catabolism via the EDP and OPPP pathways produces NADPH, which is needed in antioxidant production/regeneration. The ratio of OPPP to EDP fluxes would regulate the NADPH production rate, since the first produces two, and the second one NADPH per glucose equivalent. Immune cell oxidative attack has been shown to result in inhibition of glycolytic metabolism beyond glyceraldehyde-3-phosphate (Deng et al., 2014), perhaps favoring utilization of the EDP to bypass the lower steps of glycolysis. The gene producing glucose-6-phosphate dehydrogenase, *zwf*, normally under repression when non-glucose carbon sources are available, becomes dysregulated in some cystic fibrosis isolates (Ma et al., 1998; Silo-suh et al., 2005). It will be necessary to extend the present approach to characterizing clinical strains to determine whether the flux phenotypes and their correlates observed here also hold under conditions more closely resembling those in the CF lung.

Acknowledgments

We wish to thank Matthew Juergens for performing the Hierarchical Clustering Analysis and for the preliminary work and culturing for this project by Nathan Praschan and Raven Batshon. We also wish to thank Seattle Children's Hospital Cystic Fibrosis Isolate Core (NIH P30 DK089507) for their donation of strain AMT0023-30 and the RTSF Mass Spectrometry and Metabolomics Core for at Michigan State University for their analytical support. Michael Opperman was supported in part by funds from the Cellular and Molecular Biology Graduate Program and College of Human Medicine at Michigan State University and by a MD-Ph.D. Fellowship grant by Spectrum Health.

Appendix A. Supporting information

Supplementary data associated with this article can be found in the online version at http://dx.doi.org/10.1016/j.ymben.2016.09.002.

References

Abernathy, J., Corkill, C., Hinojosa, C., Li, X., Zhou, H., 2013. Deletions in the pyruvate pathway of Salmonella typhimurium alter SPI1-mediated gene expression and infectivity. J. Anim. Sci. Biotechnol. 4, 5. http://dx.doi.org/10.1186/2049-1891-4-5.

Adebiyi, A.O., Jazmin, L.J., Young, J.D., 2015. 13C flux analysis of cyanobacterial metabolism. Photosynth. Res. 126, 19–32. http://dx.doi.org/10.1007/s11120-014-0045-1.

Allen, D.K., Shachar-Hill, Y., Ohlrogge, J.B., 2007. Compartment-specific labeling information in 13C metabolic flux analysis of plants. Phytochemistry 68, 2197–2210. http://dx.doi.org/10.1016/j.phytochem.2007.04.010.

Alonso, a, Rojo, F., Martínez, J.L., 1999. Environmental and clinical isolates of Pseudomonas aeruginosa show pathogenic and biodegradative properties irrespective of their origin. Environ. Microbiol. 1, 421–430, doi:emi52 [pii].

Alonso, A.P., Goffman, F.D., Ohlrogge, J.B., Shachar-Hill, Y., 2007. Carbon conversion efficiency and central metabolic fluxes in developing sunflower (Helianthus annuus L.) embryos. Plant J. 52, 296–308. http://dx.doi.org/10.1111/j.1365-313X.2007.03235.x.

Alvarez-Ortega, C., Harwood, C.S., 2007. Responses of *Pseudomonas aeruginosa* to low oxygen indicate that growth in the cystic fibrosis lung is by aerobic respiration. Mol. Microbiol. 65, 153–165. http://dx.doi.org/10.1111/j.1365-2958.2007.05772.x.

Anderson, A.J., Hacking, A.J., Dawes, E.A., 1987. Alternative pathways for the biosynthesis of alginate from fructose and glucose in *Pseudomonas Mendocina* and *Azotobacter vinelandii*. Microbiology 133, 1045–1052. http://dx.doi.org/10.1099/00221287-133-4-1045.

Antoniewicz, M.R., 2013. 13C metabolic flux analysis: optimal design of isotopic labeling experiments. Curr. Opin. Biotechnol. 24, 1116–1121. http://dx.doi.org/10.1016/j.copbio.2013.02.003.

Antoniewicz, M.R., Kelleher, J.K., Stephanopoulos, G., 2006. Determination of confidence intervals of metabolic fluxes estimated from stable isotope measurements. Metab. Eng. 8, 324–337. http://dx.doi.org/10.1016/j.ymben.2006.01.004.

Baart, G.J.E., Willemsen, M., Khatami, E., de Haan, A., Zomer, B., Beuvery, E.C., et al., 2008. Modeling *Neisseria meningitidis* B metabolism at different specific growth rates. Biotechnol. Bioeng. 101, 1022–1035. http://dx.doi.org/10.1002/bit.22016.

Bell, S.C., De Boeck, K., Amaral, M.D., 2014. New pharmacological approaches for cystic fibrosis: Promises, progress, pitfalls. Pharmacol. Ther. 145, 19–34. http://dx.doi.org/10.1016/j.pharmthera.2014.06.005.

Berger, A., Dohnt, K., Tielen, P., Jahn, D., Becker, J., Wittmann, C., 2014. Robustness and plasticity of metabolic pathway flux among uropathogenic isolates of Pseudomonas aeruginosa. PLoS One 9, e88368. http://dx.doi.org/10.1371/journal.pone.0088368.

Beste, D.J.V., Nöh, K., Niedenführ, S., Mendum, T. a, Hawkins, N.D., Ward, J.L., et al., 2013. 13C-flux spectral analysis of host-pathogen metabolism reveals a mixed diet for intracellular mycobacterium tuberculosIs. Chem. Biol. 20, 1012–1021. http://dx.doi.org/10.1016/j.chembiol.2013.06.012.

Bjarnsholt, T., Jensen, P.Ø., Fiandaca, M.J., Pedersen, J., Hansen, C.R., Andersen, C.B., et al., 2009. Pseudomonas aeruginosa biofilms in the respiratory tract of cystic fibrosis patients. Pediatr. Pulmonol. 44, 547–558. http://dx.doi.org/10.1002/ppul.21011.

Borgos, S.E.F., Bordel, S., Sletta, H., Ertesvåg, H., Jakobsen, Ø., Bruheim, P., et al., 2013. Mapping global effects of the anti-sigma factor MucA in *Pseudomonas fluorescens* SBW25 through genome-scale metabolic modeling. BMC Syst. Biol. 7. http://dx.doi.org/10.1186/1752-0509-7-19.

Bowden, S.D., Ramachandran, V.K., Knudsen, G.M., Hinton, J.C.D., Thompson, A., 2010. An Incomplete TCA Cycle Increases Survival of Salmonella Typhimurium during Infection of Resting and Activated Murine Macrophages, May RC, editor. PLoS One, 5: e13871. doi:10.1371/journal.pone.0013871.

Bragonzi, A., Wiehlmann, L., Klockgether, J., Cramer, N., Worlitzsch, D., Döning, G., et al., 2006. Sequence diversity of the mucABD locus in Pseudomonas aeruginosa isolates from patients with cystic fibrosis. Microbiology 152, 3261–3269. http://dx.doi.org/10.1099/mic.0.29175-0.

Bragonzi, A., Paroni, M., Nonis, A., Cramer, N., Montanari, S., Rejman, J., et al., 2009. *Pseudomonas aeruginosa* microevolution during cystic fibrosis lung infection establishes clones with adapted virulence. Am. J. Respir. Crit. Care Med. 180, 138–145. http://dx.doi.org/10.1164/rccm.200812-1943OC.

Breidenstein, E.B.M., de la Fuente-Núñez, C., Hancock, R.E.W., 2011. Pseudomonas aeruginosa: all roads lead to resistance. Trends Microbiol. 19, 419–426. http://dx.doi.org/10.1016/j.tim.2011.04.005.

Bücker, R., Heroven, A.K., Becker, J., Dersch, P., Wittmann, C., 2014. The pyruvate-tricarboxylic acid cycle node. J. Biol. Chem 289, 30114–30132. http://dx.doi.org/10.1074/jbc.M114.581348.

Caballero, J.D., Clark, S.T., Coburn, B., Zhang, Y., Wang, P.W., Donaldson, S.L., et al., 2015. Selective sweeps and parallel pathoadaptation drive pseudomonas aeruginosa evolution in the cystic fibrosis lung. mBio 6, 1–14. http://dx.doi.org/10.1128/mBio.00981-15.

Carter, M.E.K., Fothergill, J.L., Walshaw, M.J., Rajakumar, K., Kadioglu, A., Winstanley, C., 2010. A subtype of a Pseudomonas aeruginosa cystic fibrosis epidemic strain exhibits enhanced virulence in a murine model of acute respiratory infection. J. Infect. Dis. 202, 935–942. http://dx.doi.org/10.1086/655781.

Chavarría, M., Nikel, P.I., Pérez-Pantoja, D., De Lorenzo, V., 2013. The Entner-Doudoroff pathway empowers Pseudomonas putidaKT2440 with a high tolerance to oxidative stress. Environ. Microbiol. 15, 1772–1785. http://dx.doi.org/10.1111/1462-2920.12069.

Chen, X., Shachar-Hill, Y., 2012. Insights into metabolic efficiency from flux analysis. J. Exp. Bot. 63, 2343–2351. http://dx.doi.org/10.1093/jxb/ers057.

Chen, X., Alonso, A.P., Allen, D.K., Reed, J.L., Shachar-Hill, Y., 2011. Synergy between 13C-metabolic flux analysis and flux balance analysis for understanding metabolic adaption to anaerobiosis in *E. coli*. Metab. Eng. 13, 38–48. http://dx.doi.org/10.1016/j.ymben.2010.11.004.

Cheng, K., Smyth, R.L., Govan, J.R., Doherty, C., Winstanley, C., Denning, N., et al., 1996. Spread of beta-lactam-resistant Pseudomonas aeruginosa in a cystic fibrosis clinic. Lancet 348, 639–642. http://dx.doi.org/10.1016/S0140-6736(96)05169-0.

Chokkathukalam, A., Kim, D.-H., Barrett, M.P., Breitling, R., Creek, D.J., 2014. Stable isotope-labeling studies in metabolomics: new insights into structure and dynamics of metabolic networks. Bioanalysis 6, 511–524. http://dx.doi.org/10.4155/bio.13.348.

Chung, J.C.S., Becq, J., Fraser, L., Schulz-Trieglaff, O., Bond, N.J., Foweraker, J., et al., 2012. Genomic variation among contemporary Pseudomonas aeruginosa isolates from chronically infected cystic fibrosis patients. J. Bacteriol. 194, 4857–4866. http://dx.doi.org/10.1128/JB.01050-12.

Ciofu, O., Riis, B., Pressler, T., Enghusen, H., Høiby, N., Poulsen, H.E., 2005. Occurrence of hypermutable Pseudomonas aeruginosa in cystic fibrosis patients is associated with the oxidative stress caused by chronic lung inflammation. Antimicrob. Agents Chemother. 49, 2276–2282. http://dx.doi.org/10.1128/AAC.49.6.2276.

Clark, S.T., Diaz Caballero, J., Cheang, M., Coburn, B., Wang, P.W., Donaldson, S.L., et al., 2015. Phenotypic diversity within a Pseudomonas aeruginosa population infecting an adult with cystic fibrosis. Sci. Rep. Nat. Publ. Group 5, 10932. http://dx.doi.org/10.1038/srep10932.

Cohen, T.S., Prince, A., 2012. Cystic fibrosis: a mucosal immunodeficiency syndrome. Nat. Med. Nat. Publ. Group 18, 509–519. http://dx.doi.org/10.1038/nm.2715.

Costerton, J.W., Stewart, P.S., Greenberg, E.P., 1999. Bacterial biofilms: a common cause of persistent infections. Science 284, 1318–1322. http://dx.doi.org/10.1126/science.284.5418.1318.

Cross, A., Allen, J.R., Burke, J., Ducel, G., Harris, A., John, J., et al., 1983. Nosocomial infections due to Pseudomonas aeruginosa: review of recent trends. Rev. Infect. Dis. 5 (Suppl 5), S837–S845 (Available) ⟨http://www.ncbi.nlm.nih.gov/pubmed/6361960⟩.

Crown, S.B., Long, C.P., Maciek, R., 2015. Integrated 13C-metabolic flux analysis of 14 parallel labeling experiments in *Escherichia coli*. Metab. Eng. 28, 151–158. http://dx.doi.org/10.1016/j.ymben.2015.01.001.

Dacheux, D., Epaulard, O., de Groot, A., Guery, B., Leberre, R., Attree, I., et al., 2002. Activation of the *Pseudomonas aeruginosa* type III secretion system requires an intact pyruvate dehydrogenase aceAB operon. Infect. Immun. 70, 3973–3977. http://dx.doi.org/10.1128/IAI.70.7.3973-3977.2002.

Darch, S.E., McNally, A., Harrison, F., Corander, J., Barr, H.L., Paszkiewicz, K., et al., 2015. Recombination is a key driver of genomic and phenotypic diversity in a *Pseudomonas aeruginosa* population during cystic fibrosis infection. Sci. Rep. 5, 7649. http://dx.doi.org/10.1038/srep07649.

Dash, M., Liu, H., Scheuermann, P., Tan, K.L., 2003. Fast hierarchical clustering and its validation. Data Knowl. Eng. 44, 109–138. http://dx.doi.org/10.1016/S0169-023X(02)00138-6.

De Soyza, A., Hall, A.J., Mahenthiralingam, E., Drevinek, P., Kaca, W., Drulis-Kawa, Z., et al., 2013. Developing an international Pseudomonas aeruginosa reference panel. MicrobiologyOpen 2, 1010–1023. http://dx.doi.org/10.1002/mbo3.141.

Deng, X., Liang, H., Ulanovskaya, O.A., Ji, Q., Zhou, T., Sun, F., et al., 2014. Steady-state hydrogen peroxide induces glycolysis in Staphylococcus aureus and pseudomonas aeruginosa. J. Bacteriol. 196, 2499–2513. http://dx.doi.org/10.1128/

JB.01538-14.
Dunn, M.F., Ramírez-Trujillo, J.A., Hernández-Lucas, I., 2009. Major roles of isocitrate lyase and malate synthase in bacterial and fungal pathogenesis. Microbiology 155, 3166–3175. http://dx.doi.org/10.1099/mic.0.030858-0.
Elrod, R.P., Braun, A.C., 1942. Pseudomonas aeruginosa; its role as a plant pathogen. J. Bacteriol. 44, 633–645.
Flamholz, A., Noor, E., Bar-Even, A., Liebermeister, W., Milo, R., 2013. Glycolytic strategy as a tradeoff between energy yield and protein cost. Proc. Natl. Acad. Sci. USA 110, 10039–10044. http://dx.doi.org/10.1073/pnas.1215283110.
Fothergill, J.L., Panagea, S., Hart, C. a, Walshaw, M.J., Pitt, T.L., Winstanley, C., 2007. Widespread pyocyanin over-production among isolates of a cystic fibrosis epidemic strain. BMC Microbiol. 7, 45. http://dx.doi.org/10.1186/1471-2180-7-45.
Gadsby, D.C., Vergani, P., Csanády, L., 2006. The ABC protein turned chloride channel whose failure causes cystic fibrosis. Nature 440, 477–483. http://dx.doi.org/10.1038/nature04712.
García Martín, H., Kumar, V.S., Weaver, D., Ghosh, A., Chubukov, V., Mukhopadhyay, A., et al. A Method to Constrain Genome-Scale Models with 13C Labeling Data. Maranas C.D., editor. PLOS Comput. Biol. 2015;11: e1004363. doi:⟨10.1371/journal.pcbi.1004363⟩.
Ghosh, A., Nilmeier, J., Weaver, D., Adams, P.D., Keasling, J.D., Mukhopadhyay, A., et al., 2014. A peptide-based method for 13C Metabolic Flux Analysis in microbial communities. PLoS Comput. Biol. 10, e1003827. http://dx.doi.org/10.1371/journal.pcbi.1003827.
Götz, A., Eylert, E., Eisenreich, W., Goebel, W., 2010. Carbon metabolism of enterobacterial human pathogens growing in epithelial colorectal adenocarcinoma (Caco-2) cells. PLoS One 5, 8–9. http://dx.doi.org/10.1371/journal.pone.
Hagins, J.M., Locy, R., Silo-Suh, L., 2009. Isocitrate lyase supplies precursors for hydrogen cyanide production in a cystic fibrosis isolate of Pseudomonas aeruginosa. J. Bacteriol. 191, 6335–6339. http://dx.doi.org/10.1128/JB.00692-09.
Harmer, C., Alnassafi, K., Hu, H., Elkins, M., Bye, P., Rose, B., et al., 2013. Modulation of gene expression by Pseudomonas aeruginosa during chronic infection in the adult cystic fibrosis lung. Microbiology 159, 2354–2363. http://dx.doi.org/10.1099/mic.0.066985-0.
Hauser, A.R., Jain, M., Bar-Meir, M., McColley, S. a, 2011. Clinical significance of microbial infection and adaptation in cystic fibrosis. Clin. Microbiol. Rev. 24, 29–70. http://dx.doi.org/10.1128/CMR.00036-10.
Head, N.E., Yu, H., 2004. Cross-sectional analysis of clinical and environmental isolates of pseudomonas aeruginosa: biofilm formation, virulence, and genome diversity. Infect. Immun. 72, 133–144. http://dx.doi.org/10.1128/IAI.72.1.133-144.2004.
Heux, S., Poinot, J., Massou, S., Sokol, S., Portais, J.-C., 2014. A novel platform for automated high-throughput fluxome profiling of metabolic variants. Metab. Eng. 25, 8–19. http://dx.doi.org/10.1016/j.ymben.2014.06.001.
Hoboth, C., Hoffmann, R., Eichner, A., Henke, C., Schmoldt, S., Imhof, A., et al., 2009. Dynamics of adaptive microevolution of hypermutable Pseudomonas aeruginosa during chronic pulmonary infection in patients with cystic fibrosis. J. Infect. Dis. 200, 118–130. http://dx.doi.org/10.1086/599360.
Hogardt, M., Heesemann, J., 2013. Microevolution of pseudomonas aeruginosa to a chronic pathogen of the cystic fibrosis lung. Curr. Top. Microbiol Immunol. 358, 91–118. http://dx.doi.org/10.1007/82_2011_199.
Huse, H.K., Kwon, T., Zlosnik, J.E.A., Speert, D.P., Marcotte, E.M., Whiteley, M., 2010. Parallel evolution in *Pseudomonas aeruginosa* over 39,000 generations in vivo. mBio 1. http://dx.doi.org/10.1128/mBio.00199-10.Editor.
Hyduke, D., Hyduke, D., Schellenberger, J., Que, R., Fleming, R., Thiele, I., et al., 2011. COBRA Toolbox 2.0. Protoc. Exch. . http://dx.doi.org/10.1038/protex.2011.234
Jain, C., Yun, M., Politz, S.M., Rao, R.P., 2009. A pathogenesis assay using Saccharomyces cerevisiae and Caenorhabditis elegans reveals novel roles for yeast AP-1, Yap1, and host dual oxidase BLI-3 in fungal pathogenesis. Eukaryot. Cell 8, 1218–1227. http://dx.doi.org/10.1128/EC.00367-08.
Jeukens, J., Boyle, B., Kukavica-Ibrulj, I., Ouellet, M.M., Aaron, S.D., Charette, S.J., et al., 2014. Comparative genomics of isolates of a *Pseudomonas aeruginosa* epidemic strain associated with chronic lung infections of cystic fibrosis patients. PLoS One 9, 1–15. http://dx.doi.org/10.1371/journal.pone.0087611.
Junker, B.H., 2014. Flux analysis in plant metabolic networks: increasing throughput and coverage. Curr. Opin. Biotechnol. 26, 183–188. http://dx.doi.org/10.1016/j.copbio.2014.01.016.
Karr, J.R., Takahashi, K., Funahashi, A., 2015. The principles of whole-cell modeling. Curr. Opin. Microbiol. 27, 18–24. http://dx.doi.org/10.1016/j.mib.2015.06.004.
Kavanagh, K., Reeves, E.P., 2004. Exploiting the potential of insects for in vivo pathogenicity testing of microbial pathogens. FEMS Microbiol. Rev. 28, 101–112. http://dx.doi.org/10.1016/j.femsre.2003.09.002.
Kelleher, J.K., 2001. Flux estimation using isotopic tracers: common ground for metabolic physiology and metabolic engineering. Metab. Eng. 3, 100–110. http://dx.doi.org/10.1006/mben.2001.0185.
Kerem, B., Rommens, J.M., Buchanan, J. a, Markiewicz, D., Cox, T.K., Chakravarti, A., et al., 1989. Identification of the cystic fibrosis gene: genetic analysis. Science 245, 1073–1080 (Available) ⟨http://www.ncbi.nlm.nih.gov/pubmed/2570460⟩.
Kerr, J.R., 1994. Suppression of fungal growth exhibited by Pseudomonas aeruginosa. J. Clin. Microbiol. 32, 525–527 (Available) ⟨http://www.pubmedcentral.nih.gov/articlerender.fcgi?artid=263067&tool=pmcentrez&rendertype=abstract⟩.
Kessie, T.G., 1984. Alterative pathways of carbohydrate utilization in Pseudomonads. Annu. Rev. Microbiol. 38, 359–387.
Kim, H.U., Kim, T.Y., Lee, S.Y., 2010. Genome-scale metabolic network analysis and drug targeting of multi-drug resistant pathogen Acinetobacter baumannii AYE. Mol. Biosyst. 6, 339–348. http://dx.doi.org/10.1039/b916446d.
Kim, H.U., Kim, S.Y., Jeong, H., Kim, T.Y., Kim, J.J., Choy, H.E., et al., 2014. Integrative genome-scale metabolic analysis of Vibrio vulnificus for drug targeting and discovery. Mol. Syst. Biol. Nat. Publ. Group 7. http://dx.doi.org/10.1038/msb.2010.115.
Klingner, A., Bartsch, A., Dogs, M., Wagner-Döbler, I., Jahn, D., Simon, M., et al., 2015. Large-scale 13C-flux profiling reveals conservation of the Entner-Doudoroff pathway as glycolytic strategy among glucose-using marine bacteria. Appl. Environ. Microbiol. 81. http://dx.doi.org/10.1128/AEM.03157-14.
Kohlstedt, M., Becker, J., Wittmann, C., 2010. Metabolic fluxes and beyond – systems biology understanding and engineering of microbial metabolism. Appl. Microbiol. Biotechnol. 88, 1065–1075. http://dx.doi.org/10.1007/s00253-010-2854-2.
Lagrange-Puget, M., Durieu, I., Ecochard, R., Abbas-Chorfa, F., Drai, J., Steghens, J.P., et al., 2004. Longitudinal study of oxidative status in 312 cystic fibrosis patients in stable state and during bronchial exacerbation. Pedia. Pulmonol. 38, 43–49. http://dx.doi.org/10.1002/ppul.20041.
Lamb, C., Dixon, R.A., 1997. The Oxidative Burst in. Plant Dis. Resist. Annu. Mol. Biol. 48, 251–275. http://dx.doi.org/10.1146/annurev.arplant.48.1.251.
Lambeth, J.D., 2004. NOX enzymes and the biology of reactive oxygen. Nat. Rev. Immunol. 4, 181–189. http://dx.doi.org/10.1038/nri1312.
Larocque, M., Chénard, T., Najmanovich, R., 2014. A curated C. difficile strain 630 metabolic network: prediction of essential targets and inhibitors. BMC Syst. Biol. 8. http://dx.doi.org/10.1186/s12918-014-0117-z.
Lee, D.-S., Burd, H., Liu, J., Almaas, E., Wiest, O., Barabasi, A.-L., et al., 2009. Comparative genome-scale metabolic reconstruction and flux balance analysis of multiple *Staphylococcus aureus* genomes identify novel antimicrobial drug targets. J. Bacteriol. 191, 4015–4024. http://dx.doi.org/10.1128/JB.01743-08.
Lee, D.-Y., Chung, B.K.S., Yusufi, F.N.K., Selvarasu, S., 2011. In silico genome-scale modeling and analysis for identifying anti-tubercular drug targets. Drug Dev. Res 72, 121–129. http://dx.doi.org/10.1002/ddr.20408.
Lewis, K., 2010. Persister cells. Annu. Rev. Microbiol 64, 357–372. http://dx.doi.org/10.1146/annurev.micro.112408.134306.
Lewis, N.E., Nagarajan, H., Palsson, B.O., 2012. Constraining the metabolic genotype-phenotype relationship using a phylogeny of in silico methods. Nat. Rev. Microbiol. 10, 291–305. http://dx.doi.org/10.1038/nrmicro2737.
Lien, S.K., Niedenführ, S., Sletta, H., Nöh, K., Bruheim, P., 2015. Fluxome study of Pseudomonas fluorescens reveals major reorganisation of carbon flux through central metabolic pathways in response to inactivation of the anti-sigma factor MucA. BMC Syst. Biol. 9. http://dx.doi.org/10.1186/s12918-015-0148-0.
Lindsey, T.L., Hagins, J.M., Sokol, P.A., Silo-Suh, L.A., 2008. Virulence determinants from a cystic fibrosis isolate of *Pseudomonas aeruginosa* include isocitrate lyase. Microbiology 154, 1616–1627. http://dx.doi.org/10.1099/mic.0.2007/014506-0.
Livermore, D.M., 2002. Multiple mechanisms of antimicrobial resistance in *Pseudomonas aeruginosa*: our worst nightmare? Clin. Infect. Dis. 34, 634–640. http://dx.doi.org/10.1086/338782.
Lorè, N.I., Cigana, C., De Fino, I., Riva, C., Juhas, M., Schwager, S., et al., 2012. Cystic fibrosis-niche adaptation of *Pseudomonas aeruginosa* reduces virulence in multiple infection hosts. PLoS One 7, e35648. http://dx.doi.org/10.1371/journal.pone.0035648.
Lyczak, J.B., Cannon, C.L., Pier, G.B., 2002. Lung infections associated with cystic fibrosis. Clin. Microbiol. Rev. 15, 194–222. http://dx.doi.org/10.1128/CMR.15.2.194.
Ma, J., Hager, P.W., Howell, M.L., Phibbs, P.V., Hassett, D.J., 1998. Cloning and Characterization of the Pseudomonas aeruginosa zwf Gene Encoding Enzyme Important in Resistance to Methyl Cloning and Characterization of the Pseudomonas aeruginosa zwf Gene Encoding Glucose-6-Phosphate Dehydrogenase, an Enzyme Important in R. 180, pp. 1741–1749.
Ma, L., Conover, M., Lu, H., Parsek, M.R., Bayles, K., Wozniak, D.J., 2009. Assembly and development of the Pseudomonas aeruginosa biofilm matrix. PLoS Pathog., 5. http://dx.doi.org/10.1371/journal.ppat.1000354.
Mahadevan, R., Schilling, C.H., 2003. The effects of alternate optimal solutions in constraint-based genome-scale metabolic models. Metab. Eng. 5, 264–276. http://dx.doi.org/10.1016/j.ymben.2003.09.002.
Maier, T., Güell, M., Serrano, L., 2009. Correlation of mRNA and protein in complex biological samples. FEBS Lett. Fed. Eur. Biochem. Soc. 583, 3966–3973. http://dx.doi.org/10.1016/j.febslet.2009.10.036.
Manaker, S., Tino, G., 1997. Natural history and prognosis of advanced lung disease. Clin. Chest Med. 18, 435–455, doi:10.1016.
Markussen, T., Marvig, R.L., Gomez-Lozano, M., Aanaes, K., Burleigh, A.E., Hoiby, N., et al., 2014. Environmental heterogeneity drives within-host diversification and evolution of *Pseudomonas aeruginosa*. mBio 5. http://dx.doi.org/10.1128/mBio.01592-14.
Mavrodi, D.V., Bonsall, R.F., Delaney, S.M., Soule, M.J., Phillips, G., Thomashow, L.S., 2001. Functional analysis of genes for biosynthesis of pyocyanin and phenazine-1-carboxamide from *Pseudomonas aeruginosa* PAO1. J. Bacteriol. 183, 6454–6465. http://dx.doi.org/10.1128/JB.183.21.6454.
McAtee, A.G., Jazmin, L.J., Young, J.D., 2015. Application of isotope labeling experiments and ^{13}C flux analysis to enable rational pathway engineering. Curr. Opin. Biotechnol. 36, 50–56. http://dx.doi.org/10.1016/j.copbio.2015.08.004.
McDougald, D., Rice, S. a, Barraud, N., Steinberg, P.D., Kjelleberg, S., 2011. Should we stay or should we go: mechanisms and ecological consequences for biofilm dispersal. Nat. Rev. Microbiol. Nat. Publ. Group 10, 39–50. http://dx.doi.org/10.1038/nrmicro2695.
Mena, A., Smith, E.E., Burns, J.L., Speert, D.P., Moskowitz, S.M., Perez, J.L., et al., 2008. Genetic adaptation of Pseudomonas aeruginosa to the airways of cystic fibrosis

patients is catalyzed by hypermutation. J. Bacteriol. 190, 7910–7917. http://dx.doi.org/10.1128/JB.01147-08.
Mercado-Lubo, R., Leatham, M.P., Conway, T., Cohen, P.S., 2009. Salmonella enterica Serovar Typhimurium mutants unable to convert malate to pyruvate and oxaloacetate are avirulent and immunogenic in BALB/c mice. Infect. Immun. 77, 1397–1405. http://dx.doi.org/10.1128/IAI.01335-08.
Mitchell, R.M.S., Byrne, M.F., Baillie, J., 2003. Pancreatitis. Lancet 361, 1447–1455, doi:3001.
Montezano, D., Meek, L., Gupta, R., Bermudez, L.E., Bermudez, J.C.M., 2015. Flux balance analysis with objective function defined by proteomics data-metabolism of mycobacterium tuberculosis exposed to mefloquine. PLoS One 10, e0134014. http://dx.doi.org/10.1371/journal.pone.0134014.
Mulcahy, L.R., Burns, J.L., Lory, S., Lewis, K., 2010. Emergence of *Pseudomonas aeruginosa* strains producing high levels of persister cells in patients with cystic fibrosis. J. Bacteriol. 192, 6191–6199. http://dx.doi.org/10.1128/JB.01651-09.
Neidhardt, F.C., Edwin Umbarger, H., 1996. Chemical Composition of Escherichia coli. Chem Compos Escherichia coli Neidhardt, F.C. (Ed), Escherichia coli Salmonella Cell Mol Biol, Escherichi.
Niedenführ, S., Wiechert, W., Nöh, K., 2015. How to measure metabolic fluxes: a taxonomic guide for (13)C fluxomics. Curr. Opin. Biotechnol. 34, 82–90. http://dx.doi.org/10.1016/j.copbio.2014.12.003.
Oberhardt, M. a, Goldberg, J.B., Hogardt, M., Papin, J. a, 2010. Metabolic network analysis of *Pseudomonas aeruginosa* during chronic cystic fibrosis lung infection. J. Bacteriol. 192, 5534–5548. http://dx.doi.org/10.1128/JB.00900-10.
Oberhardt, M.A., Puchałka, J., Fryer, K.E., Martins dos Santos, V. a P., Papin, J.A., 2008. Genome-scale metabolic network analysis of the opportunistic pathogen *Pseudomonas aeruginosa* PAO1. J. Bacteriol. 190, 2790–2803. http://dx.doi.org/10.1128/JB.01583-07.
Orth, J.D., Thiele, I., Palsson, B.Ø., 2010. What is flux balance analysis? Nat. Biotechnol. 28, 245–248. http://dx.doi.org/10.1038/nbt.1614.What.
Park, A.J., Murphy, K., Krieger, J.R., Brewer, D., Taylor, P., Habash, M., et al., 2014. A temporal examination of the planktonic and biofilm proteome of whole cell *Pseudomonas aeruginosa* PAO1 using quantitative mass spectrometry. Mol. Cell Proteom. 13, 1095–1105. http://dx.doi.org/10.1074/mcp.M113.033985.
Paula Alonso, A., Dale, V.L., Shachar-Hill, Y., 2010. Understanding fatty acid synthesis in developing maize embryos using metabolic flux analysis. Metab. Eng. 12, 488–497. http://dx.doi.org/10.1016/j.ymben.2010.04.002.
Pearson LIII, K., 1901. On lines and planes of closest fit to systems of points in space. Philos. Mag. Ser. 6 (2), 559–572. http://dx.doi.org/10.1080/14786440109462720.
Puchalka, J., Oberhardt, M.A., Godinho, M., Bielecka, A., Regenhardt, D., Timmis, K. N., et al., 2008. Genome-scale reconstruction and analysis of the Pseudomonas putida KT2440 metabolic network facilitates applications in biotechnology. Plos Comput. Biol. 4, e1000210. http://dx.doi.org/10.1371/journal.pcbi.1000210.
Qureshi, M.N., Perez, A.A., Madayag, R.M., Bottone, E.J., 1993. Inhibition of Acanthamoeba species by Pseudomonas aeruginosa: rationale for their selective exclusion in corneal ulcers and contact lens care systems. J. Clin. Microbiol. 31, 1908–1910 (Available) ⟨http://www.pubmedcentral.nih.gov/articlerender.fcgi?artid=265656&tool=pmcentrez&rendertype=abstract⟩.
Rau, M.H., Marvig, R.L., Ehrlich, G.D., Molin, S., Jelsbak, L., 2012. Deletion and acquisition of genomic content during early stage adaptation of Pseudomonas aeruginosa to a human host environment. Environ. Microbiol. 14, 2200–2211. http://dx.doi.org/10.1111/j.1462-2920.2012.02795.x.
Riordan, J.R., Rommens, J.M., Kerem, B., Alon, N., Rozmahel, R., Grzelczak, Z., et al., 1989. Identification of the cystic fibrosis gene: cloning and characterization of complementary DNA. Science 245, 1066–1073. http://dx.doi.org/10.1126/science.2475911.
Romano, a H., Conway, T., 1996. Evolution of carbohydrate metabolic pathways. Res. Microbiol. 147, 448–455. http://dx.doi.org/10.1016/0923-2508(96)83998-2.
Rommens, J., Iannuzzi, M., Kerem, B., Drumm, M., Melmer, G., Dean, M., et al., 1989. Identification of the cystic fibrosis gene: chromosome walking and jumping (80-). Science 245, 1059–1065. http://dx.doi.org/10.1126/science.2772657.
Ryall, B., Davies, J.C., Wilson, R., Shoemark, A., Williams, H.D., 2008. *Pseudomonas aeruginosa*, cyanide accumulation and lung function in CF and non-CF bronchiectasis patients. Eur. Respir. J. 32, 740–747. http://dx.doi.org/10.1183/09031936.00159607.
Salunkhe, P., Smart, C.H.M., Morgan, J.A.W., Panagea, S., Walshaw, M.J., Hart, C.A., et al., 2005. A cystic fibrosis epidemic strain of *Pseudomonas aeruginosa* displays enhanced virulence and antimicrobial resistance. J. Bacteriol. 187, 4908–4920. http://dx.doi.org/10.1128/JB.187.14.4908-4920.2005.
Sambrook, J., Russel, D.W., 2001. Molecular Cloning, A Laboratory Manual. Spring Harbor Laboratory Press, Cold Spring Habor, NY.
Sauer, K., Cullen, M.C., Rickard, a H., Zeef, L. a H., Gilbert, P., Davies, D.G., 2004. Characterization of nutrient-induced dispersion in *Pseudomonas aeruginosa* PAO1 BiofiLm. J. Bacteriol. 186, 7312–7326. http://dx.doi.org/10.1128/JB.186.21.7312.
Schmidt, K., Nørregaard, L.C., Pedersen, B., Meissner, A., Duus, J.Ø., Nielsen, J.Ø., et al., 1999. Quantification of intracellular metabolic fluxes from fractional enrichment and 13C–13C coupling constraints on the isotopomer distribution in labeled biomass components. Metab. Eng. 1, 166–179. http://dx.doi.org/10.1006/mben.1999.0114.
Schuetz, R., Kuepfer, L., Sauer, U., 2007. Systematic evaluation of objective functions for predicting intracellular fluxes in *Escherichia coli*. Mol. Syst. Biol., 3. http://dx.doi.org/10.1038/msb4100162.
Schwender, J., Ohlrogge, J.B., Shachar-Hill, Y., 2003. A flux model of glycolysis and the oxidative pentosephosphate pathway in developing Brassica napus embryos. J. Biol. Chem. 278, 29442–29453. http://dx.doi.org/10.1074/jbc.M303432200.
Sigurdsson, G., Fleming, R.M.T., Heinken, A., Thiele, I., 2012. A systems biology approach to drug targets in pseudomonas aeruginosa biofilm. PLoS One 7, 1–9. http://dx.doi.org/10.1371/journal.pone.0034337.
Silo-suh, L., Suh, S., Phibbs, P.V., Ohman, D.E., 2005. Adaptations of *Pseudomonas aeruginosa* to the cystic fibrosis lung environment can include deregulation of zwf, encoding glucose-6-phosphate dehydrogenase. J. Bacteriol. 187, 7561–7568. http://dx.doi.org/10.1128/JB.187.22.7561.
Son, M.S., Matthews, W.J., Kang, Y., Nguyen, D.T., Hoang, T.T., 2007. In vivo evidence of *Pseudomonas aeruginosa* nutrient acquisition and pathogenesis in the lungs of cystic fibrosis patients. Infect. Immun. 75, 5313–5324. http://dx.doi.org/10.1128/IAI.01807-06.
Song, C., Chiasson, M. a, Nursimulu, N., Hung, S.S., Wasmuth, J., Grigg, M.E., et al., 2013. Metabolic reconstruction identifies strain-specific regulation of virulence in Toxoplasma gondii. Mol. Syst. Biol. Nat. Publ. Group 9, 708. http://dx.doi.org/10.1038/msb.2013.62.
Sosnay, P.R., Siklosi, K.R., Van Goor, F., Kaniecki, K., Yu, H., Sharma, N., et al., 2013. Defining the disease liability of variants in the cystic fibrosis transmembrane conductance regulator gene. Nat. Genet. 45, 1160–1167. http://dx.doi.org/10.1038/ng.2745.
Stewart, P.S., Franklin, M.J., 2008. Physiological heterogeneity in biofilms. Nat. Rev. Microbiol. 6, 199–210. http://dx.doi.org/10.1038/nrmicro1838.
Stover, C., Pham, X., Erwin, a, Mizoguchi, S., 2000. Complete genome sequence of Pseudomonas aeruginosa PAO1, an opportunistic pathogen. Nature 406, 959–964 (Available) ⟨http://www.nature.com/nature/journal/v406/n6799/abs/406959a0.html⟩.
Toya, Y., Ishii, N., Nakahigashi, K., Hirasawa, T., Soga, T., Tomita, M., et al., 2010. 13C-Metabolic flux analysis for batch culture of *Escherichia coli* and its pyk and pgi gene knockout mutants based on mass isotopomer distribution of intracellular metabolites. Biotechnol. Prog. 26, 975–992. http://dx.doi.org/10.1002/btpr.420.
Van Alst, N.E., Picardo, K.F., Iglewski, B.H., Haidaris, C.G., 2007. Nitrate sensing and metabolism modulate motility, biofilm formation, and virulence in *Pseudomonas aeruginosa*. Infect. Immun. 75, 3780–3790. http://dx.doi.org/10.1128/IAI.00201-07.
Varga, J.J., Barbier, M., Mulet, X., Bielecki, P., Bartell, J.A., Owings, J.P., et al., 2015. Genotypic and phenotypic analyses of a Pseudomonas aeruginosa chronic bronchiectasis isolate reveal differences from cystic fibrosis and laboratory strains. BMC Genom. 16, 883. http://dx.doi.org/10.1186/s12864-015-2069-0.
Veith, N., Solheim, M., van Grinsven, K.W.A., Olivier, B.G., Levering, J., Grosseholz, R., et al., 2015. Using a genome-scale metabolic model of *Enterococcus faecalis* V583 To assess amino acid uptake and its impact on central metabolism. Appl. Environ. Microbiol. 81, 1622–1633. http://dx.doi.org/10.1128/AEM.03279-14.
Von Stockar, U., Liu, J.S., 1999. Does microbial life always feed on negative entropy? Thermodynamic analysis of microbial growth. Biochim. Biophys. Acta – Bioenerg. 1412, 191–211. http://dx.doi.org/10.1016/S0005-2728(99)00065-1.
Wagner, V.E., Iglewski, B.H., 2008. *P. aeruginosa* Biofilms in CF Infection. Clin. Rev. Allergy Immunol., 1–11. http://dx.doi.org/10.1007/s12016-008-8079-9.
Wang, C., Deng, Z.-L., Xie, Z.-M., Chu, X.-Y., Chang, J.-W., Kong, D.-X., et al., 2014. Construction of a genome-scale metabolic network of the plant pathogen *Pectobacterium carotovorum* provides new strategies for bactericide discovery. FEBS Lett. Fed. Eur. Biochem. Soc. 589, 285–294. http://dx.doi.org/10.1016/j.febslet.2014.12.010.
Wiechert, W., Möllney, M., Petersen, S., De Graaf, A.A., 2001. A universal framework for 13C metabolic flux analysis. Metab. Eng. 3, 265–283. http://dx.doi.org/10.1006/mben.2001.0188.
Wiechert, W., Möllney, M., Isermann, N., Wurzel, M., De Graaf, A., 1999. Bidirectional reaction steps in metabolic networks: III. Explicit solution and analysis of isotopomer labeling systems. Biotechnol. Bioeng. 66, 69–85. http://dx.doi.org/10.1002/(SICI)1097-0290(1999)66:2<69::AID-BIT1>3.0.CO;2-6.
Wilharm, G., Heider, C., 2014. Interrelationship between type three secretion system and metabolism in pathogenic bacteria. Front. Cell. Infect. Microbiol. 4, 1–10. http://dx.doi.org/10.3389/fcimb.2014.00150.
Williams, T.C.R., Poolman, M.G., Howden, A.J.M., Schwarzlander, M., Fell, D.A., Ratcliffe, R.G., et al., 2010. A genome-scale metabolic model accurately predicts fluxes in central carbon metabolism under stress conditions. Plant Physiol. 154, 311–323. http://dx.doi.org/10.1104/pp.110.158535.
Wu, C., Xiong, W., Dai, J., Wu, Q., 2015. Genome-based metabolic mapping and ^{13}C flux analysis reveal systematic properties of an Oleaginous microalga *Chlorella protothecoides*. Plant Physiol. 167, 586–599. http://dx.doi.org/10.1104/pp.114.250688.
Wu, X., Held, K., Zheng, C., Staudinger, B.J., Chavez, J.D., Weisbrod, C.R., et al., 2015. Dynamic proteome response of *Pseudomonas aeruginosa* to tobramycin antibiotic treatment. Mol. Cell Proteom. 14, 2126–2137. http://dx.doi.org/10.1074/mcp.M115.050161.
Yorgey, P., Rahme, L.G., Tan, M.W., Ausubel, F.M., 2001. The roles of mucD and alginate in the virulence of *Pseudomonas aeruginosa* in plants, nematodes and mice. Mol. Microbiol. 41, 1063–1076. http://dx.doi.org/10.1046/j.1365-2958.2001.02580.x.
Zamboni, N., Sauer, U., 2004. Model-independent fluxome profiling from 2H and 13C experiments for metabolic variant discrimination. Genome Biol. 5, R99. http://dx.doi.org/10.1186/gb-2004-5-12-r99.
Ziady, A.G., Hansen, J., 2014. Redox balance in cystic fibrosis. Int. J. Biochem. Cell Biol. 52, 113–123. http://dx.doi.org/10.1016/j.biocel.2014.03.006.